University of Alberta

Specific Energy Consumption (SEC) for pipeline transport of liquid CO_2 slurries

by

Rajesh Hegde

A thesis submitted to the Faculty of Graduate Studies and Research
in partial fulfillment of the requirements for the degree of

Master of Science

in

Chemical Engineering

Department of Chemical and Materials Engineering

©Rajesh Hegde
Fall 2013
Edmonton, Alberta

ABSTRACT

In this study, Specific Energy Consumption (SEC) was used as a basis to optimize the operating conditions (pipe diameter, particle size and solids concentration) for a hypothetical liquid CO_2 slurry pipeline, carrying petroleum coke ("pet coke") or sulfur particles. The optimum particle size and solids concentration were found to be 100-150μm and approximately 30% by volume respectively. Calculations of SEC involve prediction of the flowing slurry's frictional pressure gradient, obtained here using the Saskatchewan Research Council's two-layer model. However, the model and some of the correlations it contains have not yet been tested for low carrier fluid viscosities, which is the case for liquid CO_2, whose viscosity is one order of magnitude lower than water. To test the applicability of the model's kinematic friction correlation for slurries with low carrier fluid viscosities, a 50 mm (diameter) pipe loop was designed and built to test slurries of pet coke in hot water at 70^0C. The performance of the correlation gave a direct indication of the error in the SEC calculations made for liquid CO_2 slurries in industrial pipe sizes. In addition to evaluating the performance of the model's kinematic friction correlation for slurries with low carrier fluid viscosities, effort was put to improve the model's Coulombic friction estimation. As Coulombic friction estimation in the model requires knowledge of the coefficient of friction, a simple technique to measure this parameter for various particle-pipe material combinations was proposed.

TABLE OF CONTENTS

LIST OF TABLES

LIST OF FIGURES

LIST OF SYMBOLS

a correlating parameter (Equation 2.12)

A Pipe cross-sectional area

A_1, B_1 constants in Equation (2.18)

Ar Archimedes number (Equation 2.23)

C solids volume fraction

C_{max} coarse solids settled bed volume fraction

C_r coarse solids in situ volume fraction

C_{vd} coarse solids delivered volume fraction

d particle diameter (m)

d_{50} median particle diameter (m)

d_{50c} coarse median particle diameter (m)

d^+ dimensionless particle diameter (Equation 2.20)

D Pipe diameter (m)

$\dot{E}$ Power (W)

f Fanning friction factor (Equation 2.6)

f_b Fanning friction factor for a Bingham fluid (Equation 2.10)

f_f Darcy friction factor (Equation 5.1)

f_s solids friction factor (Equation 2.17)

F Friction force (N)

Fr Froude number

g acceleration due to gravity (m/s^2)

He Hedstrom number (Equation 2.13)

i_m hydraulic gradient (m fluid/m pipe)

k Pipe hydrodynamic roughness (m)

L length of rheometer spindle (m)

M Solids mass flow rate (kg/s)

P Pressure (Pa)

Q Volumetric flow rate (m^3/s)

R radius of rheometer spindle or cup (m)

Re Reynolds number (Equation 2.8)

Re_b Reynolds number for a Bingham fluid (Equation 2.11)

S Wetted perimeter (m)

S_s Specific gravity

SEC Specific Energy Consumption (kWh.tonne^{-1}.km^{-1})

v_∞ terminal settling velocity of a single particle (m/s)

V bulk velocity (m/s)

V_c deposition velocity (m/s)

V_t threshold turbulent velocity (m/s)

T torque (N.m)

z horizontal distance in pipeline (m)

Greek Symbols

β half-angle subtended by lower layer in the SRC model

δ viscous sublayer thickness (m)

η_s coefficient of sliding friction

λ linear concentration (Equation 2.19)

μ Newtonian viscosity (Pa·s)

μ_p Bingham plastic viscosity (Pa·s)

ρ density (kg/m^3)

τ_w wall shear stress (Pa)

τ_f wall shear stress associated with the flow of carrier fluid (Pa)

τ_k kinematic contribution to wall shear stress (Pa)

τ_0 Bingham yield stress (Pa)

τ_s wall shear stress associated with the flow of solids (Pa)

ω rotational spindle speed (radian/s)

Subscripts

f carrier fluid

m mixture, or slurry

p particle

s solids

1 Introduction

1.1 Motivation

Rapid expansion of the Canadian oil sands industry has led to a significant increase in greenhouse gas (GHG) emissions, in particular carbon dioxide (CO_2), to the atmosphere, according to Environment Canada. In a recent report (**Environment Canada**, **2012)**, it has been projected that the current GHG emissions from oil sand operations will nearly double by 2020. As the International Energy Agency has stated that GHG emissions are the primary cause of climate change, the projected emission trend from oil sands operations should be a cause for concern. For a large-scale reduction in industrial CO_2 emissions, Carbon Capture and Storage (CCS) is one of the feasible mitigation strategies, which involves capturing CO_2 from industrial point sources and transporting it to storage sites (saline aquifers and rock formations) or enhanced oil recovery (EOR) sites (**Wilson and Monea, 2004**). The main obstacle for commercial deployment of CCS is that the operations involved are expensive. For instance, it has been estimated that an investment of $1 to $3 billion per year will be required from the governments of Alberta and Canada to promote CCS projects, apart from significant additional investment from the industry itself (**Alberta CCS Development Council, 2009**).

In CCS, large quantities of CO_2 need to be transported over long distances from the capture site to the storage site. Under this scenario, pipelines offer the most

economical and efficient way to transport CO_2, as they provide continuous flow without any need of intermediate storage facilities, unlike road or rail transport. For pipeline transport, CO_2 in liquid form is preferred over gaseous form (**Zhang et al., 2006**). This is because transporting CO_2 in gaseous state is disadvantageous, as its low density means that less CO_2 is transported per unit volume. If liquid CO_2 is transported, the possibility of conveying value-added commodities like petroleum coke or sulfur in slurry form exists, and could be used to improve the economics of CCS (**Luhning, 2010**). These solids are byproducts from the oil sand upgrading process and a recent report (**Energy Resources Conservation Board, 2012**) suggests that inventories of pet coke have been rising steadily over the past decade. In the same report, sulfur recovery from bitumen upgrading has been forecasted to go up by 56% in 2021 as compared to that in 2001. Also, the report notes petroleum coke's commercial value as a fuel and the usage of sulfur in the phosphate fertilizer industry. Therefore, both commodities are valuable and readily available for transport to markets. In this initiative, illustrated in Figure 1.1, these solids coming out of the upgrading process will be mixed with liquid CO_2, obtained from compression of gaseous CO_2 emitted from the same upgrader plant. The resulting slurry will then be transported by pipeline. At the end point of this pipeline, the solid products will be separated from CO_2 and delivered to awaiting markets by rail, while the liquid CO_2 will be sent to storage sites for sequestration. This entire process is expected to generate additional income for the industry from the sale of sulfur and/or pet coke, thereby offsetting a portion of the total cost of CCS. Apart from reducing

costs in CCS, this initiative will promote the movement and sale of these value-added commodities, which are currently being stored or disposed of at the oil sands plant sites. Presently, transportation of these solids to markets is hampered by the isolation of the producers from rail terminals. An overview of the CO_2 slurry pipeline routing in this initiative can be found in **Luhning (2012)**. The CO_2 slurry pipeline could originate in Fort McMurray, Alberta and run as far as Swan Hills, Alberta. Solids would be separated from the liquid CO_2 stream at that location and would be transferred to the rail service south of Swan Hills, while liquid CO_2 could be sent to the oil fields in Swan Hills and Pembina, both located in Alberta, for enhanced oil recovery application. Further details and benefits of this initiative are given elsewhere (**Luhning, 2010**).
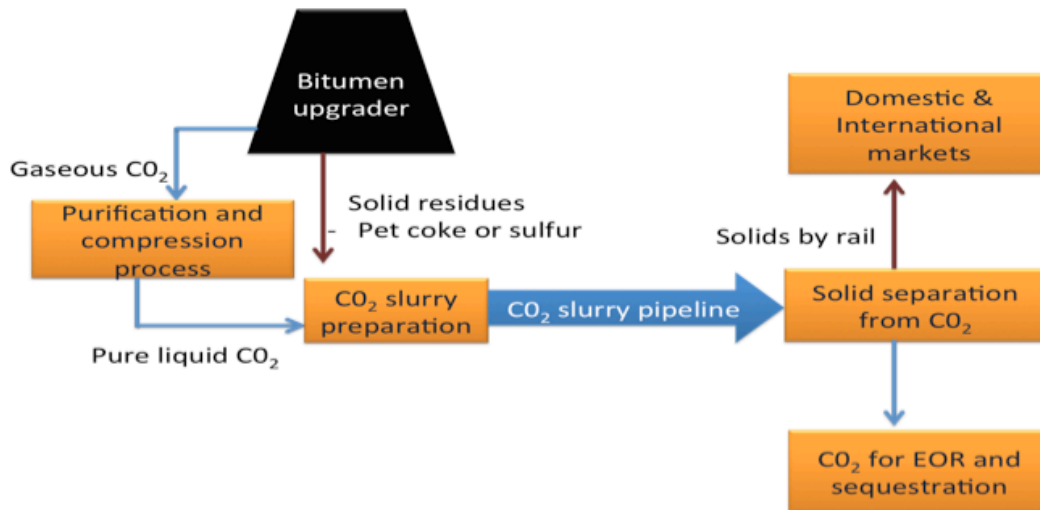
Figure 1.1 Schematic overview of the CO_2 slurry pipeline initiative for the oil sands industry

The design of a CO_2 slurry pipeline is one of the major components in the implementation of this initiative. Within the overall pipeline design process, our

3

focus is on the pipeline hydraulic design. One of the important design criteria in the hydraulic design of slurry pipelines is the calculation of Specific Energy Consumption (SEC), which represents the energy required to transport a unit mass of solids per unit length of pipe. In other words, SEC is a good indicator of the energy efficiency of a slurry (solids-in-liquid) pipeline. An analysis of this type helps in selecting the optimum pipeline operating conditions for energy efficient slurry transportation. Specifically, the effects of pipe diameter, flow velocity, particle size and solids concentration on the power requirements of a slurry pipeline can be evaluated using the SEC concept. This study provides a detailed SEC analysis for liquid CO_2 slurry pipelines to optimize the aforementioned operating conditions. In the future, pipeline engineers can use the SEC analysis from this study for planning, commissioning and constructing an industrial or pilot scale liquid CO_2 slurry pipeline.

The details of the SEC analysis, which are given in Chapter 2, show that the slurry frictional pressure gradient (frictional pressure loss per unit pipeline length) for a given set of operating conditions is a critical input. Additionally, the slurry frictional pressure gradient is needed to estimate total pressure loss and determine the number of pumps required. It is worth noting here that a SEC calculation is dependent on the slurry frictional pressure gradient for a given set of operating conditions. Hence, an accurate estimation of friction loss for liquid CO_2 slurries is critical to the overall hydraulic design of a liquid CO_2 slurry pipeline. However, the literature provides almost no data or even an indication of the most reliable

4

model for estimating CO_2 slurry friction losses. In the 1980's, **Santhanam (1983)** and **Ng and Bhattacharya (1988)** studied the friction loss behavior of very fine particles ($d_{50}<44\mu m$) of coal in liquid CO_2. Their work cannot be extended to account for friction loss behavior of coarser particles transported in liquid CO_2. This is explained in greater detail in Chapter 2 (Background). In this application, however, particles of either petroleum coke or sulfur will be coarse (d_{50} in the range of 100-150μm). The justification for this particle size range can be understood from the SEC analysis presented in Chapter 3.

In the pipeline flow of coarse-particle (settling) slurries, as in the case of the liquid CO_2 slurries that are the focus of this study, particles contribute friction in ways that cannot be described by fluid-like (viscosity) models, and will accumulate in the pipeline if it is operated below a minimum velocity required to suspend the solids. In other words, particles increasingly stratify with decreasing flow velocity and below a critical velocity called the "deposition velocity" (V_c), a stationary deposit of solids forms on the bottom of the pipeline. If the nominal mixture velocity (Q/A) is further decreased below the deposition velocity, the height of the stationary bed increases, which can lead to pipeline plugging. For slurries of this type, the flow must be turbulent and the minimum operating velocity is kept slightly higher than deposition velocity. It is worth noting here that the mixture deposition velocity is different from the terminal settling velocity of a single particle in a quiescent fluid. In the horizontal pipe flow of coarse-particle slurries, the turbulent fluctuation velocity should be higher than the

terminal settling velocity to avoid deposition of the solids (**Davies, 1987**). As the turbulent fluctuation velocity is a small component of the mean flow velocity, the mixture deposition velocity is always higher than the terminal settling velocity of a single particle. To date, the best model to predict friction losses and deposition velocities for settling slurries is the Saskatchewan Research Council's (SRC) two-layer model (**Gillies et al., 1991; Shook and Roco, 1991; Shook et al., 2002; Gillies et al., 2004, Spelay et al., 2013**). It is a semi-mechanistic, phenomenological (force balance) model that accounts for the effects of particle diameter, solids concentration, pipe diameter and operating velocity in a physically meaningful way. The model identifies two governing friction loss components in settling slurries (**Shook et al., 2002**):

1. Kinematic friction, which is a combination of fluid-like friction of the carrier fluid and the shear-related friction from the suspended particles;
2. Coulombic friction that occurs from the sliding of the fraction of particles that are not effectively suspended by fluid turbulence.

The kinematic friction is velocity dependent, unlike the Coulombic friction component and this can be understood from the development of the model, as shown in Section 2.3. For the range of particle sizes of petroleum coke or sulfur important for this study, kinematic friction will be dominant. It should be noted that the SRC two-layer model includes a limited number of correlations, but one (Equation 2.18) is used to predict the kinematic friction component of the slurry. This correlation has not yet been tested for slurries where the carrier fluid

viscosity is in the range of that expected for liquid CO_2, which has a viscosity of about 0.1 mPa.s (one order of magnitude lower than that of water) at the typical operating temperature and pressure of a liquid CO_2 pipeline (refer to Section 2.4). Hence, the model's kinematic friction prediction is uncertain for liquid CO_2 slurries with such low carrier fluid viscosities. It needs to be mentioned here that SEC calculations for liquid CO_2 slurries in this study are done using friction loss predictions from the SRC two-layer model. Therefore, to determine if our SEC calculations are reasonable, it is necessary to validate the model's kinematic friction correlation for slurries having low carrier fluid viscosities by producing new experimental friction loss data. These data will give a direct indication of the error in the SEC calculations presented as part of this study.

To this end, an experimental program was designed to acquire friction loss data from the pipe flow tests of coarse particle slurries with low carrier fluid viscosities. In this program, a 50mm slurry pipe loop was designed, fabricated and commissioned to test slurries of petroleum coke (d_{50} =128μm) in hot water (i.e. 70^0C). Here, 70^0C water was chosen as a model fluid for liquid CO_2, because it has a kinematic viscosity similar to that of liquid CO_2. It was much less experimentally challenging and more economical to use this model fluid instead of liquid CO_2 for the pipe loop tests, as explained in greater detail in Section 2.4. The experimental friction loss data from the pet coke-hot water tests are used to evaluate the performance of the SRC model's kinematic friction correlation for slurries with low carrier fluid viscosities and also to evaluate the error (if any) in

the SEC analysis presented here. As the kinematic friction loss correlation is essentially independent of pipe diameter, any observations or trends taken from the 50mm loop tests of this study should be applicable to industrial pipe sizes.

The range of solids concentrations tested for the pet coke-hot water slurries in the 50mm loop covers the optimum or most economical solids concentration for transportation of liquid CO_2 slurry in industrial pipe sizes.

It is worth mentioning here that sulfur-hot water slurries were not tested in the 50mm loop due to the possibility that severe corrosion of the pipe material (stainless steel) could occur. A previous study (**Kadry, 2008)** indicated that stainless steel pipe is susceptible to sulfide stress corrosion cracking in the temperature range of 60-100^{0}C and formation of H_2S can occur from acidification of water with elemental sulfur (**Fang et al., 2008**). Further investigation of the corrosion of stainless steel by sulfur-hot water mixtures through the use of bench scale tests is warranted before one could safely test slurries of this type in the loop described in the present study.

In addition to evaluating the performance of the SRC model's kinematic friction correlation for slurries with low carrier fluid viscosities, a part of this study involves improving the Coulombic friction loss estimation capability of the SRC model. The model requires the input of the coefficient of sliding friction (η_s) in estimating the Coulombic friction component (refer to Equation 2.15). Currently

in the model, determination of η_s is based on the default value of $\eta_{s0}=0.5$ (for sand slurries in steel pipes). Hence, to make the model more rigorous through the development of a database of η_{s0} values for various particle-pipe material combinations, a simple technique to measure η_{s0} is proposed. Details of this technique can be found in Section 5.5.

1.2 Objectives

The objectives of this study are:

1. To perform SEC calculations to determine the optimum operating conditions for a liquid CO_2 slurry pipeline.

2. To measure pipeline frictional pressure gradients of a model liquid CO_2 slurry (128μm pet coke in water at 70^0C) and use these data to validate the performance of the kinematic friction correlation embedded in the SRC two-layer model for slurries having low carrier fluid viscosities.

3. To use the experimental data and evaluation of the kinematic friction correlation to quantify the degree of error (if any) in the SEC calculations.

1.3 Thesis structure

The theory and the background for this research are described in detail in Chapter 2. In this Chapter, the workings of the SRC two-layer model are briefly discussed and the applicability of the model for slurries with low carrier fluid viscosities is analyzed. Selection of an analogue for liquid CO_2 is also presented at the end of Chapter 2. The SEC analysis of liquid CO_2 slurries is presented in Chapter 3. The experimental pipe loop setup and its operating procedures, along with the relevant laboratory tests, are described in Chapter 4. The experimental results and a

discussion of these results are presented in Chapter 5. The conclusions and recommendations for future work are presented in Chapter 6.

2 Background

2.1 Specific Energy Consumption

Specific Energy Consumption (SEC) for the pipeline transportation of solids can be defined as the energy required to transport a unit mass of solids over a unit length of the pipe. The SEC (J.kg^{-1}.m^{-1}) is calculated as follows:

$$SEC = \frac{\dot{E}}{M_S L} = \frac{(-\frac{dP}{dz})}{\rho_s C_{vd}} \qquad (2.1)$$

where $\dot{E}$ is the power consumption (W), M_s is the solids mass flow rate (kg/s), L is the pipe length (m), (-dP/dz) is the slurry frictional pressure gradient (Pa/m), C_{vd} is the delivered volumetric solids concentration (v/v) and ρ_s is the solids density (kg/m^3). In some of the previous studies (**Wilson et al., 2006; Pullum and McCarthy,1993**) SEC is calculated in kWh.tonne^{-1}.km^{-1}. This unit conversion is achieved by changing the SI units of power consumption, solids mass flow rate and pipe length into to their new units, which results in the division of Equation 2.1 by a factor of 3.6. In slurry pipeline transport studies, the slurry frictional pressure gradient is usually expressed as a hydraulic gradient, i_m (m fluid/m pipe). This is because, using hydraulic gradients, it becomes convenient to compare slurry friction loss across different operating conditions and the friction losses of two different slurries (different solids) prepared with the same carrier fluid. The expression for hydraulic gradient is:

$$i_m = \frac{(-\frac{dP}{dz})}{\rho_f g} \qquad (2.2)$$

where ρ_f is the density of the carrier fluid and g is the gravity constant.

On substituting (–dP/dz) in Equation 2.1 with i_m from Equation 2.2, putting the numerical value of the gravity constant in Equation 2.1 and by finally dividing Equation 2.1 by the value of 3.6, we obtain the expression for SEC in kWh/tonne-km as:

$$SEC = \frac{2.73\, i_m}{S_s * C_{vd}} \qquad (2.3)$$

where S_s is the specific gravity of the solids. It should be noted that the delivered solids concentration (C_{vd}) in Equations 2.1 or 2.3 refers to the coarse solids concentration discharged at the exit of the pipeline, which is presumably equal to the solids concentration fed to the pipeline, in other words Q_s/Q_m.

Fundamentally, SEC can be explained as the energy consumption associated with the transport of solids for a given pipe diameter, flow velocity, particle size and solids concentration. Therefore, the most energy efficient pipeline operation condition occurs at the minimum SEC. As the minimization of SEC is dependent on the aforementioned operating parameters, it is necessary to first understand variation of SEC with a single parameter, while keeping the other parameters constant. Before the discussion of these trends is presented, the basis for the SEC calculations and the focus of the present study are outlined. All SEC calculations

and figures shown in this thesis are performed using Equation 2.3, with i_m obtained from SRC two-layer model (Pipe Flow 10) predictions. The list of input parameters in the SRC model to obtain i_m is shown in Table 2.1. Appendix C contains the values of these input parameters to obtain i_m predictions for all of the SEC figures discussed in this thesis. For greater detail on the model appearance, outputs and input parameters, refer to the screen shot of Pipe Flow 10 provided in Appendix C. The workings of the SRC two-layer model are explained in detail in Section 2.3.

Table 2.1 List of inputs in the SRC model for SEC analysis

Input parameters in the SRC model
Pipe internal diameter (m)
Pipe wall roughness (mm)
Pipeline slope (degrees)
Coarse solids mass median particle diameter (mm)
Coarse solids density (kg/m^3)
Coarse solids concentration (delivered)
Coarse solids settled bed concentration
Carrier fluid density (kg/m^3)
Carrier fluid viscosity (mPa.s)

Among the input parameters shown in Table 2.1, the focus is on determining the optimum coarse solids particle size and delivered solids concentration for the evaluation of minimum SEC for liquid CO_2 slurries, as presented in Chapter 3.

13

Here, SEC trends are illustrated using a sand-water slurry, for which the mean particle diameter is taken to be constant. The trends discussed here are for flow velocities above the minimum operating velocity (deposition velocity, V_c) for any given slurry. The trend of SEC with pipe diameter is illustrated in Figure 2.1, where SEC is plotted against pipe diameter for a 174μm sand-in-water slurry at 19^0C for C_{vd}=0.20 and for V=1.1V_c. This figure illustrates that SEC decreases with increasing pipe diameter and that SEC changes only slightly at larger pipe diameters. The result from Figure 2.1 is consistent with previous studies: **Wu et al. (2006)** analyzed 90μm sand-in-water slurry data from **Schaan et al. (2000)**, whose sand in water slurry tests were conducted in nominal pipe sizes of 50 and 150 mm for various solids concentrations. **Pullum and McCarthy (1993)** surveyed various slurry flow data sets from previous publications and plotted SEC against pipe diameter for those data sets. They also observed the flattening of the SEC curve at higher pipe diameters, similar to the predicted trend shown in Figure 2.1.

The trend of SEC with flow velocity is illustrated in Figure 2.2, where SEC is plotted for a 174μm sand-in-water slurry in a 250mm pipe for two delivered solids concentrations. Here, SEC shows an increasing trend with flow velocity. Both the curves are shown to terminate at the deposition velocity of 2.9 m/s. The increasing flow velocities in Figure 2.2 correspond to increasing volumetric flow rates as the cross-sectional area available for flow (or pipe diameter) is constant.
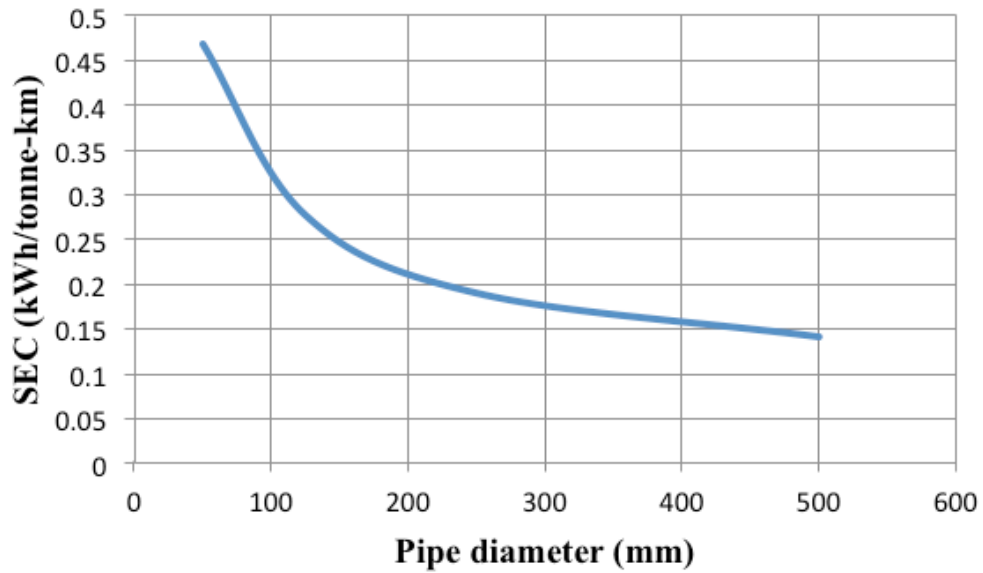
Figure 2.1 Predicted variation of SEC with pipe diameter for a sand-water slurry: $d_{50c}=174\mu m$; $T= 19^0C$; $C_{vd}=0.20$; $V= 1.1V_c$
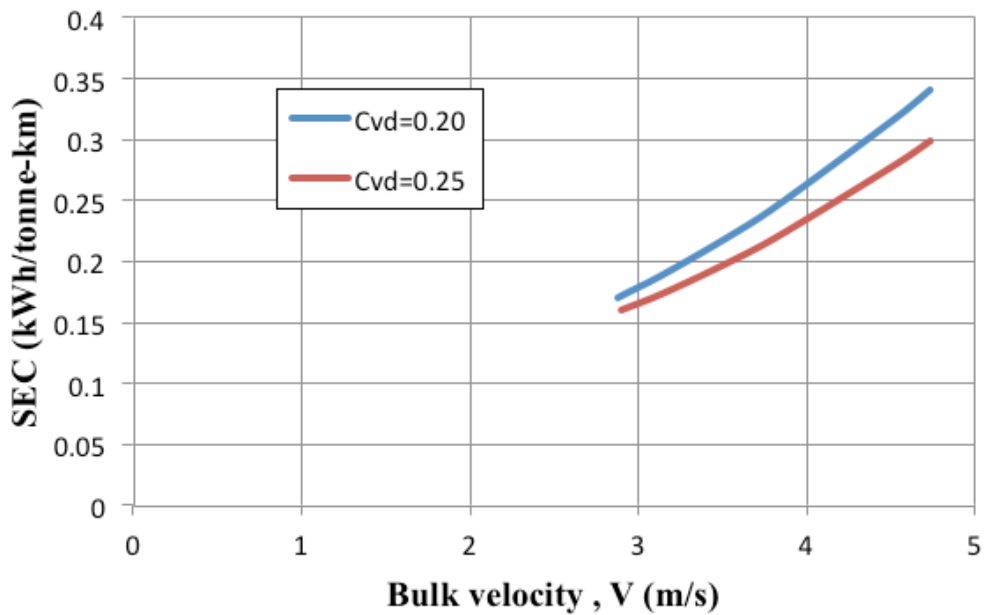
Figure 2.2 Predicted variation of SEC with flow velocity for a sand-water slurry: $D= 250mm$; $d_{50c}=174\mu m$; $T= 19^0C$

For operation below the deposition velocity (i.e. V<V$_c$) the frictional pressure gradient increases with decreasing velocity due to the increase in flow resistance arising from the increasing height of the stationary bed. Therefore, the minimum SEC is at or near V$_c$ for any settling slurry, regardless of pipe diameter and solids concentration. In actual industrial practice, operating velocities of V=1.1 to 1.3V$_c$ are typical (**Wilson et al., 2006**), with the lowest value chosen to have a margin of safety above V$_c$ to avoid deposition. Hence, V=1.1V$_c$ was taken as the basis for Figure 2.1 and will be taken as the basis for calculations in Chapter 3, where the selection of the optimum particle size and solids concentration for a pet coke-liquid CO_2 slurry pipeline is described through SEC analysis. In addition, the typical effects of flow velocity and particle diameter on SEC will be described in detail in Chapter 3.

The following section presents the theory behind friction loss prediction for so-called homogeneous slurries and reviews the literature on pipe flow studies of liquid CO_2 slurries. In Section 2.3, the workings of the SRC two-layer model are discussed and the model's applicability to liquid CO_2 slurries is analyzed.

2.2   Homogeneous, liquid CO_2-based slurries: a review

2.2.1   Introductory remarks

The mechanical energy balance for a section of pipe with constant diameter, carrying an incompressible fluid under steady state condition can be written as:

$$\frac{dP}{dz} + \rho g \frac{dh}{dz} + \frac{\tau_w S}{A} = 0 \tag{2.4}$$

The three terms in the above equation represent the pressure, gravitational and frictional contributions. For a horizontal pipe, the second term in the above equation can be eliminated. By expressing the wetted perimeter (S) and cross sectional area (A) of a cylindrical pipe in terms of pipe diameter (D) we obtain:

$$-\frac{dP}{dz} = \frac{4\tau_w}{D} \qquad (2.5)$$

Hence, the wall shear stress (τ_w) inside a horizontal pipe gives a direct measurement of the frictional pressure gradient. For the turbulent flow of a Newtonian fluid such as water, the friction factor (f) can be estimated from the pipeline Reynolds number and from the pipe wall roughness using a correlation such as that of **Churchill (1977)**. Knowing the Fanning friction factor (f), fluid velocity (V) and fluid density (ρ), the wall shear stress can be calculated using:

$$\tau_w = 0.5 f \rho V^2 \qquad (2.6)$$

For the pipeline flow of slurries, the method used to determine the friction losses differs, and the preferred method depends on whether the slurry can be considered to be homogeneous or settling (**Shook et al., 2002**). In homogeneous slurries, particles are very fine (typically $d_{50}<44\mu m$ if the particle density is $2650kg/m^3$) and are uniformly suspended in the pipe at all flow velocities. The presence of the particles augments the density and changes the viscosity/rheology of the suspending liquid. Hence, such slurries can be considered as a pseudo-continuous phase with an effective mixture density and viscosity and fluid models are appropriate to describe their friction losses. Homogeneous slurries are further

17

classified into Newtonian and non-Newtonian and their friction loss estimation methods are discussed in Sections 2.2.2 and 2.2.3 respectively. For settling slurries, which are the focus of this study, particles contribute friction in ways that cannot be described by fluid-like models and thus the notion of slurry viscosity becomes meaningless for such slurries. The SRC two-layer model is used to determine friction losses for such slurries and this model is described in detail in Section 2.3.

2.2.2   Friction losses for homogeneous, Newtonian slurries

Historically, the slurry viscosity approach proposed by **Wasp et al. (1970)** was used to determine the wall shear stress for Newtonian homogeneous slurries:

$$\tau_w = 0.5 f_m \rho_m V^2 \qquad (2.7)$$

In the above equation, ρ_m is the density of the mixture and f_m is the mixture's Fanning friction factor and is a function of the mixture Reynolds number, Re_m. The mixture Reynolds number is given as:

$$Re_m = \frac{DV\rho_m}{\mu_m} \qquad (2.8)$$

where μ_m is the slurry viscosity and all other variables have their usual meanings. For homogeneous Newtonian slurries, the particles do not flocculate and their viscosity is invariant with shear rate. Various reliable correlations are available in the literature to estimate the mixture viscosity (in Equation 2.8) for such slurries, notably the one proposed by **Thomas (1965)**:

$$\frac{\mu_m}{\mu_f} = 1 + 2.5C + 10.05C^2 + 0.00273e^{16.6C} \qquad (2.9)$$

18

In the above correlation, μ_f is the viscosity of the suspending liquid and C is the solids volume fraction in the mixture. Unfortunately, the method can give very poor predictions for turbulent pipe flow (**Gillies, 2012**). Although it is useful in explaining the concept of a homogeneous slurry, its usage for calculations is not recommended.

2.2.3 Friction losses for homogeneous, non-Newtonian slurries

In homogeneous non-Newtonian slurries, fine particles interact with each other to form flocs and either the aggregation or breakdown of the flocs with shear results in non-Newtonian behaviour. It is necessary to ascertain carefully the rheology of a non-Newtonian mixture before pipeline friction losses are calculated. Based on the rheology, a suitable fluid model that fits the rheological data needs to be selected. Numerous such models are available (**Shook et al., 2002**), but a commonly used model is the Bingham fluid model. Several approaches are found in the literature to calculate turbulent friction losses for homogeneous slurries exhibiting Bingham fluid behaviour. A common method is that proposed by Wilson and Thomas (**Shook et al., 2002**). Another approach is based on a friction factor correlation for Bingham fluids proposed by **Darby et al. (1992)**:

$$f_B = \frac{10^a}{Re_B{}^{0.193}}$$

(2.10)

where Re_B is the modified Reynolds number based on the Bingham plastic viscosity (μ_p) and mixture density ρ_m:

$$Re_B = \frac{DV\rho_m}{\mu_p}$$

(2.11)

The correlating parameter 'a' is defined in terms of the Hedstrom number:

$$a = -1.47\big(1 + 0.146(-2.9 \times 10^{-5} He)\big) \qquad (2.12)$$

where

$$He = \frac{D^2 \rho_m \tau_0}{\mu_p} \qquad (2.13)$$

where τ_o is the yield stress of the mixture.

From Equations 2.10 to 2.13, it can be seen that the friction factor is calculated with the knowledge of the rheological parameters for the Bingham fluid under consideration. Using this friction factor, turbulent friction losses can then be calculated using Equation 2.7, where f_m is replaced by f_B.

2.2.4 Previous studies involving liquid CO_2-based slurries

From 1977-1983, A. D. Little Inc and W.R. Grace & Company jointly developed the concept of transporting coal/liquid CO_2 slurries to eliminate the use of water as the carrier fluid for moving coal in pipelines. **Santhanam (1983)** studied the flow of coal-liquid CO_2 slurry in a 50mm pipe loop, with slurrying and de-slurrying units running in batch mode. Subbituminous and lignite coal with very fine particle sizes ($d_{80} \sim 88\mu m$) were used for his studies. A centrifugal pump capable of delivering flow rates corresponding to mixture velocities of 1.5 to 4.7 m/s was used to circulate the slurry in the loop. The pipe loop was operated at temperatures of 0 to 25^0C. Through the pilot tests, the effects of flow on the physical properties of the coal, loop startup/shutdown, emergency response to pipeline rupture and slurry rheology were investigated. His work was quite important as it provided proof-of-concept, showing that the transportation of

liquid CO_2 slurries was feasible. He provided a detailed description of the process technology for the slurrying and de-slurrying operations in pressurized systems, as in the case of liquid CO_2 slurry pipe loops.

Through his pilot tests, Santhanam found coal-liquid CO_2 slurries to behave rheologically as non-Newtonian fluids with Bingham plastic characteristics. Interestingly, from the pilot loop tests, Santhanam suggested that coal-liquid CO_2 slurries with a solids concentration of 80% by mass (70% by volume) have friction losses similar to water flowing alone at identical conditions. Santhanam did not publish his pipe loop data in the form of measured pressure loss vs velocity. He presented instead the rheological parameters of this slurry, as deduced from his pipe loop data, in **Santhanam et al. (1984)**. The rheological data from Santhanam et al. (1984) for 80% coal-liquid CO_2 slurry are shown in Table 2.2. Although the researchers did not explicitly state their deduction method to obtain these rheological parameters from their pipe loop data, it appears that they used correlations similar to the ones given by **Darby et al. (1992)**.

Table 2.2 Deduced rheological parameters of a 80% coal-liquid CO_2 slurry (by mass) (Santhanam et al., 1984)

Particle size d_{80} (μm)	Carrier fluid density (kg/m^3)	Mixture density (kg/m^3)	Bingham plastic viscosity (mPa.s)	Yield stress (Pa)
88	820	1210	8.5	3.5

The data from Table 2.2 can be used with any available method to calculate the turbulent friction losses for a Bingham fluid (see Section 2.2.3). It is then possible to compare these losses to those predicted for water at 19^0C. Figure 2.3 shows the comparison of the predicted hydraulic gradient (i_m) for the 80% coal-liquid CO_2 slurry obtained using the **Darby et al. (1992)** correlation for flow in a 50mm pipe with that of water at 19^0C obtained using the Churchill correlation (**Churchill, 1977**). Except at higher velocities, it can be seen that the hydraulic gradients are similar, as suggested by Santhanam.
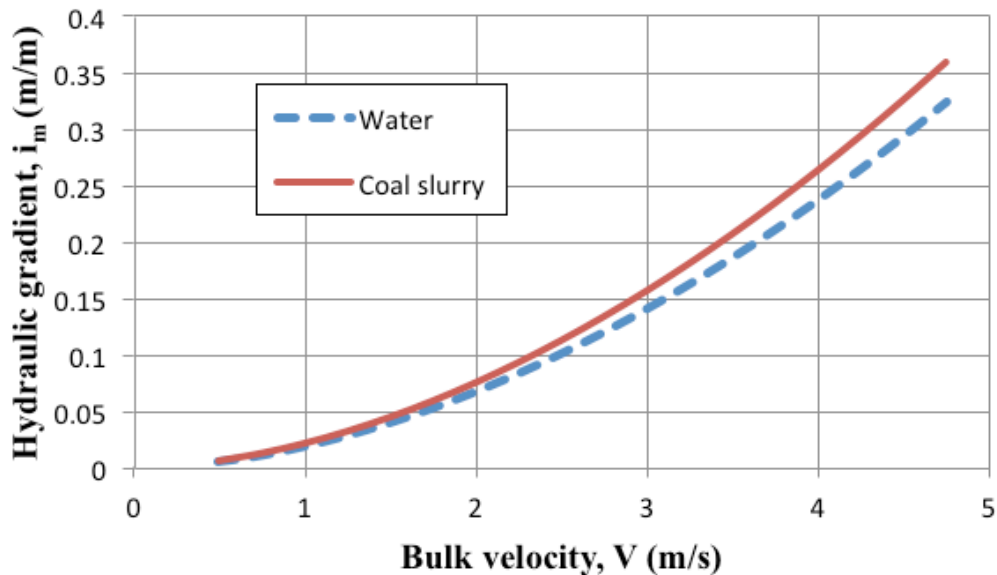
Figure 2.3 Comparison of predicted hydraulic gradients for a 80% (w/w) coal-liquid CO_2 slurry with predicted hydraulic gradients of water at 19^0C; D=50mm.

In another study by **Ng and Bhattacharya (1988)**, two brown coal samples with different moisture content (each having d_{50} ~10 μm) were tested with liquid CO_2 in a tube flow rheometer. The solids concentration was varied from 33 to 49% by

volume. They reported dilatant non-Newtonian fluid behaviour for these slurries, which is different from the Bingham fluid behaviour observed by Santhanam. The difference in rheological behaviour of liquid CO_2 slurries between the studies of **Santhanam et al. (1984) and Ng and Bhattacharya (1988)** can be attributed to a number of factors, including a difference in the coal rank (or carbon content) being tested in each study. Differences in the coal rank can result in different particle-carrier fluid chemistry, resulting in different rheology (**Yuchi et al., 2005)**.

In the previous studies of liquid CO_2 suspensions, the slurry systems under consideration were homogeneous and the slurry rheology was required to describe the friction losses of the slurries. Unfortunately, this approach cannot be extended to liquid CO_2 slurries containing larger particles, which are of interest in the present study. These slurries cannot be considered to be homogeneous. Unlike in homogeneous slurries, there are two governing particle-related friction loss mechanisms in settling slurries, i.e., the kinematic and Coulombic friction loss components. For liquid CO_2 slurries containing larger particles, the relative contribution of these components to the overall slurry friction needs to be determined for a given particle size range under consideration. Also, the coarse particles will accumulate at the pipe bottom if the flow velocity is below the deposition velocity. Hence, the more mechanistic approach provided by the SRC two-layer model must be used to obtain friction loss predictions and deposition velocities for liquid CO_2 slurries containing coarse particles. In the following

23

section, the SRC two-layer model is described and its applicability for predicting turbulent pipeline friction losses and deposition velocities for coarse-particle liquid CO_2 slurries is analyzed.

2.3   The SRC two-layer model

The conceptual basis of this model is illustrated in Figure 2.4, where the pipe cross-section is divided into two hypothetical layers with each layer approximated to have a uniform concentration and velocity. In the upper layer, particles are assumed to be fully suspended by fluid turbulence resulting in only kinematic friction or velocity-dependent friction. In the bottom layer, a fraction of the particles is assumed to be suspended by turbulence and the remaining fraction of particles is supported through contact with the pipe wall. As a result, both kinematic and Coulombic friction exist in the bottom layer (**Gillies et al., 1991; Shook and Roco, 1991; Shook et al., 2002; Gillies et al., 2004, Spelay et al., 2013**).
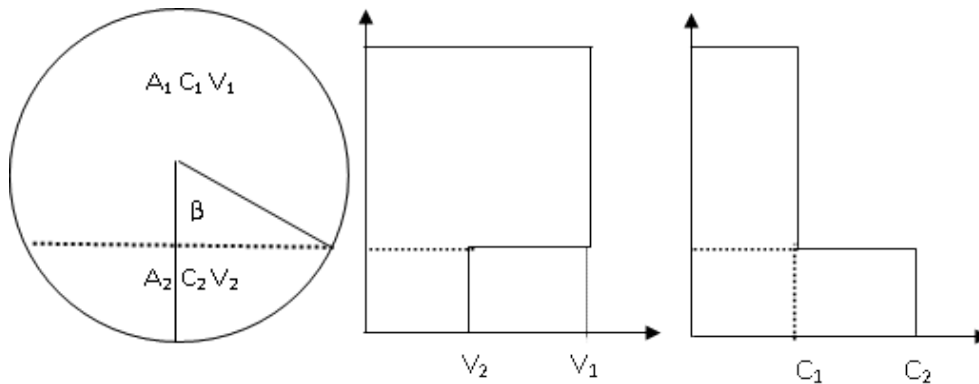
Figure 2.4 Idealized concentration and velocity distributions used in the SRC two-layer model (Gillies et al., 2004)

Steady state force and material balances are applied to each layer and the resulting set of equations is solved iteratively to provide the pressure gradient (-dP/dz). It is important to understand the force balances underlying the model as they involve computation of the Coulombic and kinematic friction components of the overall friction losses. For a horizontal slurry pipe flow, solving the force balance equations for each layer, we obtain the slurry's frictional pressure gradient:

$$-\frac{dP}{dz} = \frac{\tau_{1k}S_1 + \tau_{12}S_{12}}{A_1} \qquad (2.14a)$$

$$-\frac{dP}{dz} = \frac{\tau_{2k}S_2 - \tau_{12}S_{12} + F_2}{A_2} \qquad (2.14b)$$

where, τ_{1k}, τ_{2k} are the kinematic friction components in each layer, τ_{12} is the interfacial shear stress between the two layers, F_2 is the Coulombic friction component in the lower layer, S_1 and S_2 are the partial perimeters of the two layers and S_{12} is the partial perimeter of the interface of the two layers. The interfacial shear stress (τ_{12}) is proportional to the square of the difference between the velocities of the two layers. The Coulombic friction component (F_2) in Equation 2.14 is derived analytically (**Wilson, 1976**):

$$F_2 = 0.5\eta_s D^2 g\left(\rho_s - \rho_f\right)(C_2 - C_1)(sin\beta - \beta cos\beta) \qquad (2.15)$$

where β is defined by the cross-sectional area of the lower layer, A_2 (see Figure 2.4) and η_s is the coefficient of sliding friction. Here, η_s can be defined as the ratio of the sliding friction force of the particles on a given pipe surface to the normal (immersed) weight of the particles. Measurement of η_s is discussed in greater detail in Section 5.5. The concentrations in each layer are denoted C_1 and C_2. A

correlation for contact load fraction (C_c) is used to evaluate the difference between C_2 and C_1 (**Gillies and Shook, 2000**). The contact load fraction, C_c, is defined as:

$$C_c = \frac{A}{A_2}(C_2 - C_1) \tag{2.16}$$

The kinematic friction components (τ_{1k}, τ_{2k}) in Equation 2.14 are modeled as follows (**Shook et al., 2002**):

$$\tau_k = \tau_f + \tau_s = 0.5 f_f \rho_f V^2 + 0.5 f_s \rho_s V^2 \tag{2.17}$$

where f_f is the Fanning friction factor for the carrier fluid and f_s is the solids friction factor and is determined using the following empirical correlation (**Gillies, 2012**):

$$f_s = \lambda^{1.25}[A_1 ln(d^+) + B_1] \tag{2.18}$$

where for $d^+ \leq 21$:

$$A_1 = -1.1 \times 10^{-4} \ and \ B_1 = 4.2 \times 10^{-4} \tag{2.18a}$$

For $d^+ > 21$:

$$A_1 = -5.6 \times 10^{-5} \ and \ B_1 = 2.6 \times 10^{-4} \tag{2.18b}$$

In Equation 2.18, λ is the linear solids concentration defined with respect to the settled bed concentration (C_{max}) as:

$$\lambda = [(C_{max}/C_r)^{1/3} - 1]^{-1} \tag{2.19}$$

and d^+ is the dimensionless particle diameter, defined as:

$$d^+ = \frac{d(f_f/2)^{0.5} V \rho_f}{\mu_f}$$

(2.20)

To solve Equations 2.14 to 2.20 in the model, mixture velocity (V) or flow rate, pipe diameter (D), pipe roughness, coarse solids volume fraction (C_{vd}), settled bed concentration (C_{max}), solids density (ρ_s), coarse particle median diameter (d_{50}), carrier fluid density (ρ_f) and viscosity (μ_f) are used as input parameters. The carrier fluid viscosity is either known or measured. More details on the development of the model can be found in **Gillies et al., (1991, 2004)** and **Gillies and Shook (2000).**

The usefulness of this model can be understood from the following two factors. The model accounts for the friction loss mechanisms of coarse-particle slurries in a physically meaningful way and has limited empirical correlations (kinematic friction correlation and contact load fraction correlation). Additionally, these correlations were developed from a large experimental database of slurry tests conducted in pipe diameters ranging from 50 mm to 500mm, for average particle sizes from 0.085mm to 2.4mm and solids concentrations up to 46% by volume (**Gillies et al., 1991; Gillies et al., 2004; Gillies and Shook, 2000)**. The empirical correlations in the model are independent of pipe diameter, making the model applicable to pipes of any diameter. Therefore this model has become widely used for predicting friction losses in the turbulent flow of settling slurries, especially in the industrial hydraulic design of slurry pipelines carrying oil sand, coal, iron ore concentrates, copper tailings, etc.

The model may give inaccurate friction loss predictions if used outside the range of the experimental database (pipe diameter excluded). With regards to applicability of the model for friction loss predictions of liquid CO_2 slurries, the range of particle sizes and solids concentrations already tested for the model is sufficient. However the kinematic friction correlation (Equation 2.18) was developed using slurry friction loss data based on carrier fluid viscosities substantially greater than that of liquid CO_2 (0.1 mPa.s), which has a viscosity one order of magnitude lower than that of water. The carrier fluid viscosities already tested in the model include water at room temperature, water at 50^0C, glycol-water mixtures and clay-water mixtures (**Gillies and Shook, 2000; Gillies, 2012; Gillies, 2003**).

The performance of the kinematic friction correlation in the model may be suspect for such a low carrier fluid viscosity. Therefore, new experimental friction loss data are required to validate this correlation for settling slurries with low carrier fluid viscosities. The objective of the experimental program in the present study is to obtain friction loss data for slurry tests with petroleum coke in a low-viscosity carrier fluid (hot water at 70^0C) in a 50mm test loop and then use the data to evaluate Equation 2.18 in the model. The data will also strengthen the existing database for coarse particle (settling) slurries.

2.4 Deposition velocity predictions for liquid CO$_2$ slurries

The model also predicts the deposition velocity, V$_c$, from a force balance of the sliding bed of particles at incipient deposition condition (**Wilson, 1979**). The force balance results in the following expression for V$_c$:

$$V_c = Fr\sqrt{gD(S_s - 1)} \tag{2.21}$$

where S$_s$ is the specific gravity of the solids (ρ_s/ρ_f) and Fr is a Froude number, which is correlated with the Archimedes number as follows (**Shook et al., 2002**):

$$Fr = 1.78Ar^{-0.019}, \qquad\qquad Ar > 540 \tag{2.22a}$$

$$Fr = 1.19Ar^{0.045}, \qquad 160 < Ar < 540 \tag{2.22b}$$

$$Fr = 0.197Ar^{0.4}, \qquad 80 < Ar < 160 \tag{2.22c}$$

The Archimedes number is defined in Equation 2.23 and can be thought of as the ratio of the gravitational forces on the particle to the viscous forces acting on the particle:

$$Ar = \frac{4gd^3(\rho_s - \rho_f)\rho_f}{3\mu_f^2} \tag{2.23}$$

The model considers Archimedes number (Ar) as the principal independent variable in predicting deposition velocity for slurries as this allows the deposition velocity to be calculated over a range of particle and carrier fluid properties in non-dimensional form. The Archimedes number was calculated for the slurries of interest, i.e. liquid CO$_2$ slurries and hot water slurries to determine if the deposition velocity correlation in the model is applicable for these slurries. The

calculated Archimedes number and the physical properties for the aforementioned slurries are tabulated in Table 2.3.

Table 2.3 Archimedes number for low viscosity slurry systems

Slurry system	d_{50} (μm)	ρ_s (kg/m^3)	ρ_f (kg/m^3)	μ_f (mPa.s)	Ar
Pet coke-liquid CO_2	150	1600	867	0.1	2803
Sulfur-liquid CO_2	150	2000	867	0.1	4332
Pet coke-water at 70^{0}C	128	1600	977	0.39	110

In Table 2.3, the density of liquid CO_2 was obtained from **Duschek et al. (1990)** and the viscosity of liquid CO_2 was deduced from **Fenghour et al. (1998)**. It can be seen from Table 2.3 that the Archimedes numbers for liquid CO_2 slurries and for the pet coke-hot water slurry fall in the span of Equation 2.22a and Equation 2.22c respectively. Therefore, for slurries with low carrier fluid viscosities in general, the deposition velocity prediction from the model can be taken with confidence and the correlations do not need further validation. In this experimental program, deposition velocities predicted by the model were used as a reference to obtain minimum operating velocities for the slurry tests conducted using the 50mm loop at 20^{0}C and 70^{0}C.

2.5   Selection of an analogue for liquid CO_2

A minimum pressure of 7.38MPa is required for stable operation with liquid CO_2 in a pipe loop and to avoid phase transition to gaseous CO_2 (**McCoy and Rubin, 2008**). This pressure is significantly higher than 0.1 MPa (atmospheric pressure). Therefore, operating a liquid CO_2-based slurry loop in a laboratory environment raises operational and safety challenges. For example, inadvertent operation of pressure relief valves in the loop could result in the formation of dry ice on the valve components, causing embrittlement and leading to breakage (**Barrie et al., 2004**). Also for high pressure operating conditions required for liquid CO_2, the cost of the experiments is much higher due to the requirement of specialized materials of construction and equipment having the appropriate pressure rating.

In view of the aforementioned issues, it was decided to make the task of performing pipe loop tests less difficult and more economical by selecting a model carrier fluid whose physical properties (density and viscosity) at atmospheric pressure resemble those of liquid CO_2. For the selection, reference density and viscosity values of liquid CO_2 were taken at 17^0C and 9 MPa from **Duschek et al. (1990)** and **Fenghour et al. (1998)** respectively. This set of conditions was chosen as representative of the typical temperature and pressure range ($0-27^0C$, 7.5-20 MPa) found in an industrial liquid CO_2 pipeline (**Li, 2008**). Hot water at 70^0C approximates these requirements and was chosen as the model carrier fluid. Comparison of the physical properties of liquid CO_2 and hot water is presented in Table 2.4. Although there is some difference between the physical properties of hot water and liquid CO_2, the friction loss behaviour of their slurries

is not expected to be very different and the friction loss data obtained from hot water slurries is the simplest step forward to understand the friction loss behaviour of slurries with low carrier fluid viscosities. It is worth mentioning that other model fluids such as triethylamine were also considered. Triethylamine at room temperature has similar density and viscosity to liquid CO_2. However, as triethylamine is a flammable solvent, extensive safety measures would be needed for loop operation.

Table 2.4 Comparison of physical properties of liquid CO_2 and hot water

Carrier fluids	Temperature (^{0}C)	Pressure (MPa)	Density (kg/m^3)	Viscosity (mPa.s)
Liquid CO_2	17	9	867	0.1
Hot water	70	0.1	977	0.39

3 SEC Analysis for Liquid CO_2 Slurries

This Chapter contains the detailed SEC analysis for selecting the optimum particle size, solids concentration and flow velocity for both pet coke-liquid CO_2 slurry and sulfur-liquid CO_2 slurry in the hypothetical pipeline. The sizing of this hypothetical pipeline is done based on the anticipated volume of CO_2 to be transported. Details on the sizing can be found in the latter part of this chapter. Based on the SEC analysis for pet coke-liquid CO_2 slurries, test conditions are selected for the pet coke-hot water tests in the 50mm loop.

Since SEC is based on slurry hydraulic gradient predictions obtained with the SRC model, it is useful to analyze some hydraulic gradient (friction loss) plots for liquid CO_2 slurries before evaluating the optimum particle size and solids concentration for these slurries. This exercise will help in understanding the SEC trends obtained here for liquid CO_2 slurries. For all the hydraulic gradient plots, three particle sizes (fine: 75μm, intermediate: 128μm, coarse: 300μm) are chosen. This particle size range helps to illustrate the two governing friction loss mechanisms in settling slurries (kinematic and Coulombic friction) and also helps in justifying the eventual selection of the optimum particle size. For plots of hydraulic gradient as a function of mixture velocity or as a function of coarse solids volume fraction (C_{vd}), a pipe diameter of 200mm is chosen so that the results from these plots can be directly used to explain SEC trends in the 200mm hypothetical pipeline for liquid CO_2 slurries. For plots of hydraulic gradient as a function of mixture velocity or as a function of pipe diameter, C_{vd}=0.30 is taken

as the basis. This is done as the optimum solids concentration has been found to be near this value for settling slurries with similar particle sizes (**Hashemi et al., 2010**). Table 3.1 summarizes the input parameters used for obtaining i_m predictions (from the SRC model) for the SEC analysis done in this chapter.

Table 3.1 Input parameters and their values to obtain i_m predictions for SEC analysis

Input parameters	Values
Pipe internal diameter (mm)	50-500
Pipe wall roughness (mm)	0.01
Pipeline Slope (degrees)	0
Mixture velocity (m/s)	0.8-5
Coarse solids particle size (μm)	75-1000
Coarse solids density (kg/m^3)	1600 (pet coke) 2000 (sulfur)
Coarse delivered solids concentration	0.15-0.40
Solids settled bed concentration	0.61 (for both pet coke and sulfur)
Carrier fluid density (kg/m^3)	867 (liquid CO_2) 977 (hot water)
Carrier fluid viscosity (mPa.s)	0.1 (liquid CO_2) 0.39 (hot water)

The predicted variation of hydraulic gradient with mixture velocity is shown in Figure 3.1, for a pet coke-liquid CO_2 slurry for the three particle sizes (75μm, 128μm, 300μm) in a pipe diameter of 200mm and for C_{vd}=0.30. For any particle size, it can be seen that the slurry hydraulic gradient increases non-linearly with

34

flow velocity. Consequently, a similar trend is also observed in the variation of SEC with mixture velocity, as was seen in Figure 2.2 in the previous chapter. With the increase in flow velocity, the kinematic friction component becomes dominant over the Coulombic friction component due to improved turbulent suspension of the particles. Hence, the force balance equations in the SRC model (Equation 2.14) include only the kinematic friction component, so the wall shear stress or the hydraulic gradient varies with the square of flow velocity. In Figure 3.1, the upward shift of the hydraulic gradient curve for 300μm slurry in comparison with the finer particles is due to the greater effect of Coulombic friction for coarser particles. Also, the slight dip in the hydraulic gradient curve for the 300μm slurry can be attributed to the decrease in Coulombic friction that occurs when the flow velocity is increased beyond the deposition velocity. As the velocity continues to increase, the hydraulic gradient increases as the kinematic friction component becomes dominant. The implication of the dip in the hydraulic gradient for coarser particles is that the optimum velocity for such particles is higher than the typical optimum velocity (near V_c) for finer particles.
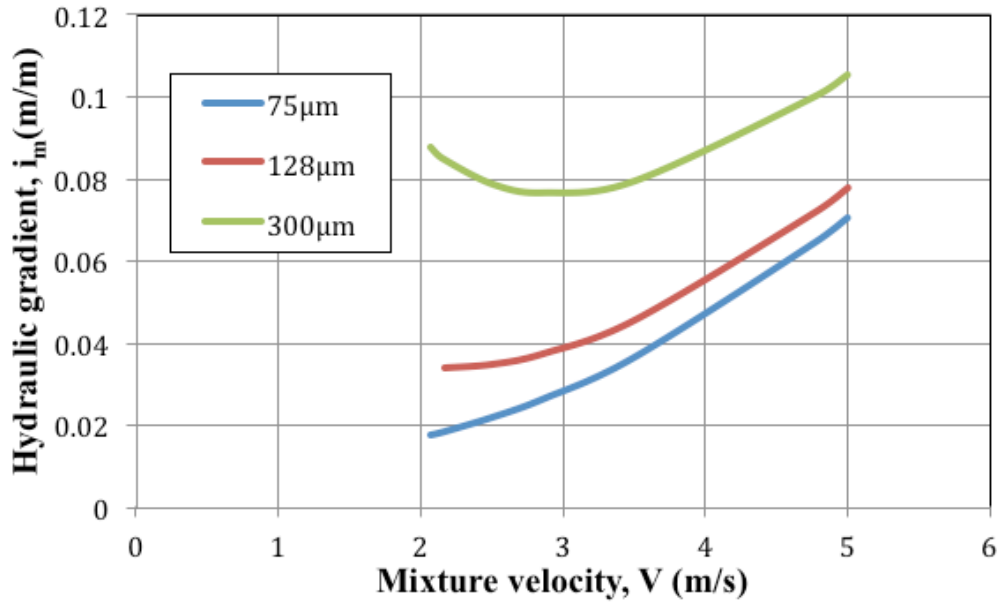
Figure 3.1 Predicted variation of hydraulic gradient with mixture velocity for a pet coke-liquid CO_2 slurry: D=200mm and C_{vd}=0.30

Figure 3.2 shows the variation of predicted hydraulic gradients with mixture velocity for a sulfur-liquid CO_2 slurry for the same three particle sizes (75μm, 128μm, 300μm) in a pipe diameter of 200mm and for C_{vd}=0.30. The trends observed here are similar to those seen in Figure 3.1. However, under the same operating conditions, the hydraulic gradient values are higher for sulfur-liquid CO_2 slurry as compared with pet coke-liquid CO_2 slurry since the density of sulfur is greater than that of pet coke. As a result, SEC values for sulfur-liquid CO_2 slurry will be higher as compared with pet coke-liquid CO_2 slurry under the same operating conditions. The proportional effect of solids density on the slurry hydraulic gradient can be understood from the particle kinematic friction model in the SRC model (Equation 2.17).
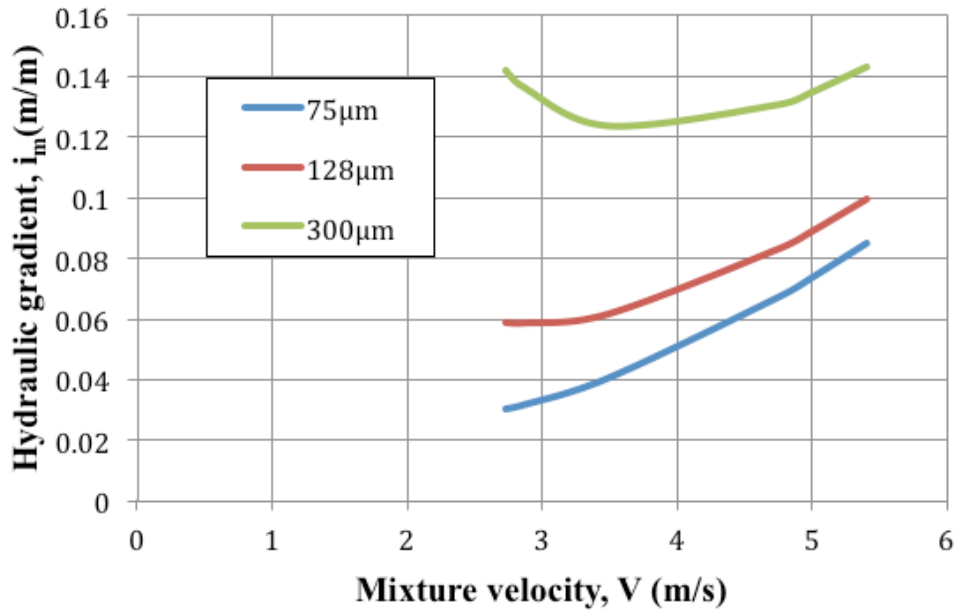
Figure 3.2 Predicted variation of hydraulic gradient with mixture velocity for a sulfur-liquid CO_2 slurry: D=200mm and C_{vd}=0.30

The predicted variation of hydraulic gradient with solids concentration (C_{vd}) for liquid CO_2 slurries is shown in Figure 3.3, for a pet coke-liquid CO_2 slurry for the three particle sizes (75µm, 128µm, 300µm) in a pipe diameter of 200mm and at V=V_c. The hydraulic gradient rise is rapid for the coarser particle slurry due to the significant Coulombic friction found at higher concentrations and near the deposition condition. For any given particle size, the non-linear variation of hydraulic gradient with solids concentration holds for higher flow velocities as well. This is due to the non-linear dependence of kinematic friction on solids volume fraction, as seen from Equation 2.18. It is interesting to note here that the plot of SEC vs. C_{vd} will not have the same trend as in the plot of i_m vs. C_{vd}, as seen in Figure 3.3, and this will be explained later in this section.

37
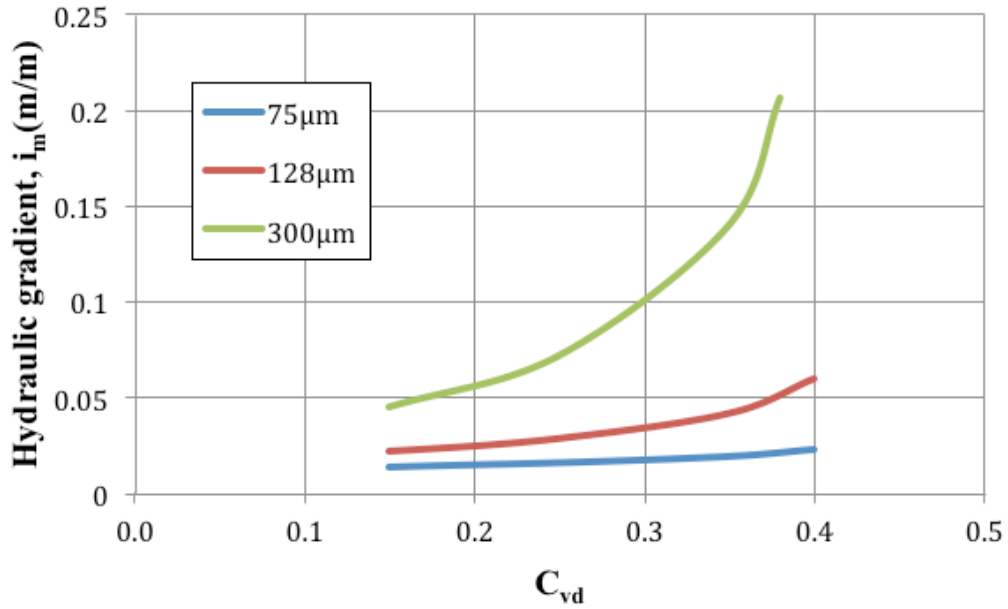
Figure 3.3 Predicted variation of hydraulic gradient with delivered solids volume fraction for a pet coke-liquid CO_2 slurry: D=200mm and V=V$_c$.

Figure 3.4 shows the variation of predicted hydraulic gradients with delivered solids volume fraction for a sulfur-liquid CO_2 slurry for the three particle sizes (75μm, 128μm, 300μm) in a pipe diameter of 200mm and at V=V$_c$. The trends here are similar to those found in Figure 3.3. As mentioned before, for the same particle size and solids concentration, the hydraulic gradient values are higher for a sulfur-liquid CO_2 slurry than for a pet coke-liquid CO_2 slurry under identical operating conditions.
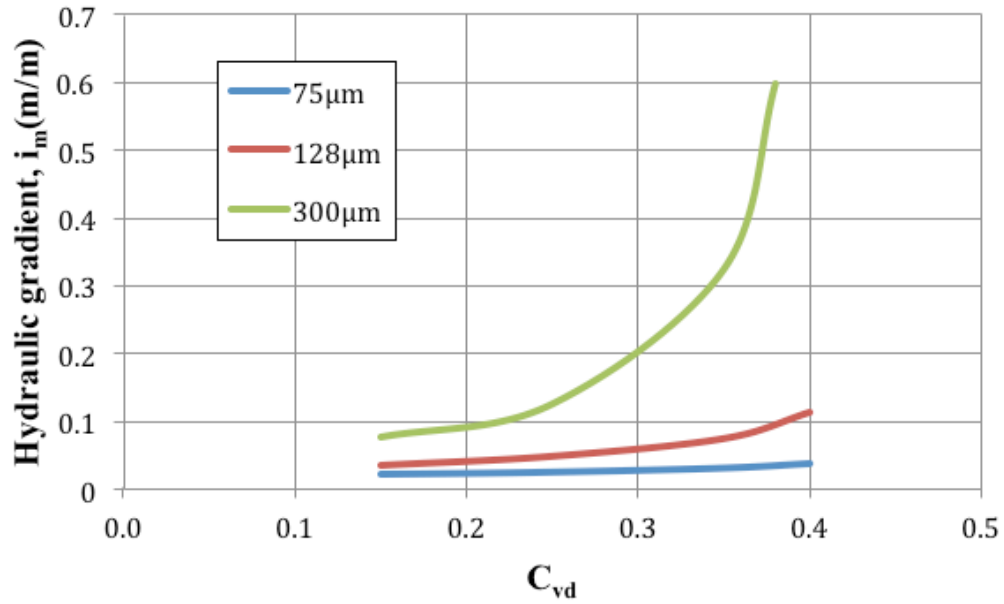
Figure 3.4 Predicted variation of hydraulic gradient with delivered solids volume fraction for a sulfur-liquid CO_2 slurry: D=200mm and V=V$_c$.

The predicted variation of hydraulic gradient with pipe diameter is shown in Figure 3.5, for a pet coke-liquid CO_2 slurry for the three particle sizes (75µm, 128µm, 300µm) at C$_{vd}$=0.30 and for V=V$_c$.
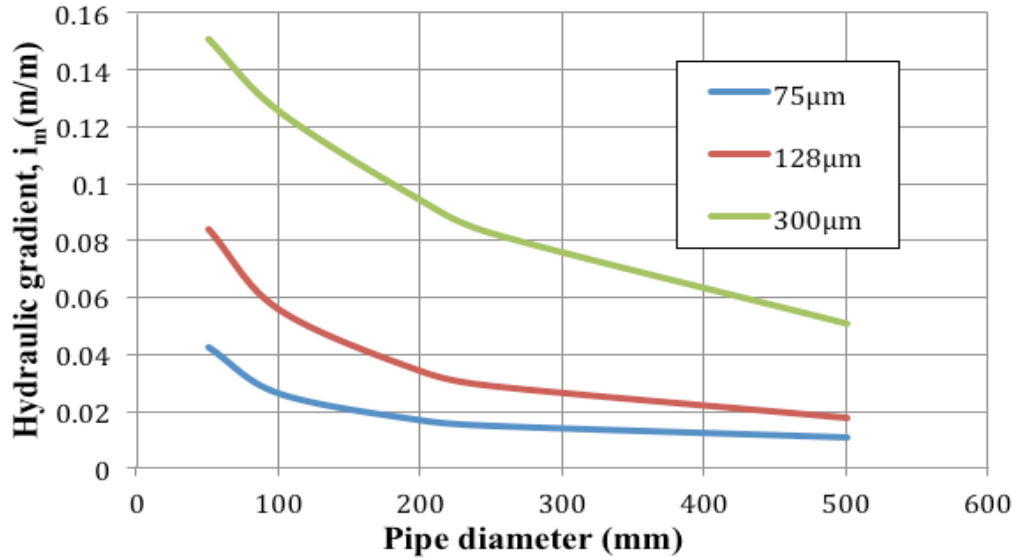
Figure 3.5 Predicted variation of hydraulic gradient with pipe diameter for a pet coke-liquid CO_2 slurry: C_{vd}=0.30 and $V=V_c$.

For single-phase flows, it is well established that the hydraulic gradient decreases with increasing pipe diameter at constant velocities and this trend is also seen for settling slurry flows from Figure 3.5. Although the Coulombic friction component in the model increases with pipe diameter (see Equation 2.15), the kinematic friction component of the slurry reduces more rapidly, causing the overall hydraulic gradient to decrease with increasing pipe diameter. The reduction in the kinematic friction component with increasing pipe diameter can be attributed to the reduction in the inter-particle dispersive stress with increase in flow cross-sectional area. Although not shown here, an analysis of the effect of pipe diameter on the hydraulic gradient for higher mixture velocities shows the same trend as in Figure 3.5. The result from Figure 3.5 accounts for the decrease of SEC with increasing pipe diameter, as was seen in Figure 2.1 in the previous chapter. The

trend of decreasing hydraulic gradient with increasing pipe diameter is also illustrated for sulfur-liquid CO_2 slurries in Figure 3.6, where predicted hydraulic gradients are plotted versus pipe diameter for the three particle sizes (75μm, 128μm, 300μm) at C_{vd}=0.30 and for V=V_c.
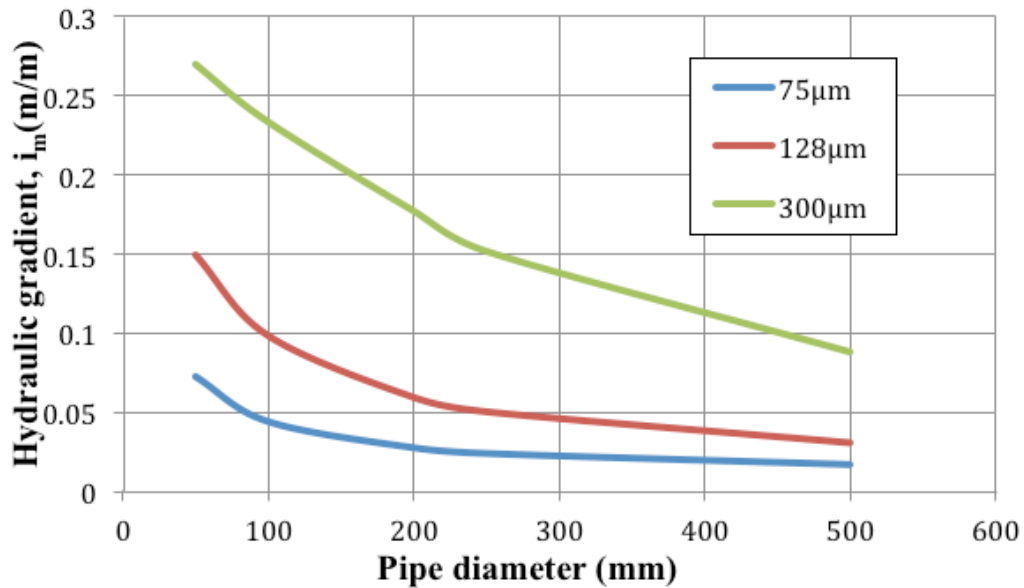
Figure 3.6 Predicted variation of hydraulic gradient with pipe diameter for a sulfur-liquid CO_2 slurry: C_{vd}=0.30 and V=V_c.

The predicted variation of deposition velocity with pipe diameter for liquid CO_2 slurries is shown in Figure 3.7, for a pet coke-liquid CO_2 slurry for the three particle sizes (75μm, 128μm, 300μm).
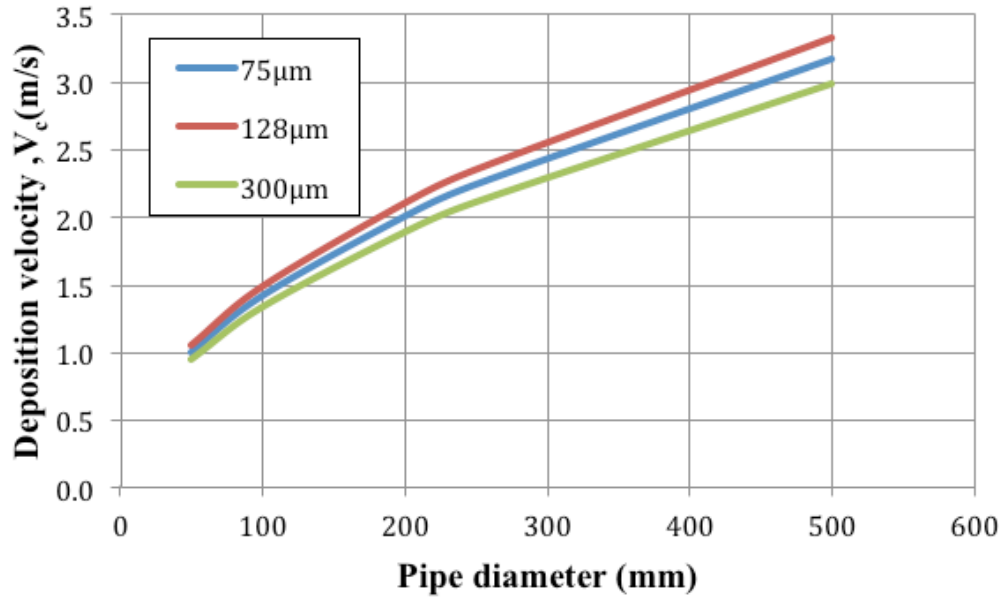
Figure 3.7 Predicted variation of deposition velocity with pipe diameter for a pet coke-liquid CO_2 slurry.

It can be seen that for any settling slurry with a given average coarse particle size, the deposition velocity, V_c, varies with the square root of the pipe diameter (see Equation 2.21). The same trend of deposition velocity with pipe diameter is also illustrated for sulfur-liquid CO_2 slurries in Figure 3.8, where predicted deposition velocities are plotted versus pipe diameter for the three particle sizes (75μm, 128μm, 300μm).

It is notable that for a 200mm pipe, the deposition velocity is approximately 2m/s for pet coke slurries and approximately 2.5m/s for sulfur slurries. This is related to the fact that liquid CO_2 is not a particularly good medium for particle suspension. For water at 20^0C, for example, $V_c=0.6$m/s for the 75μm pet coke particles and 0.85m/s for the 128μm pet coke particles.

42
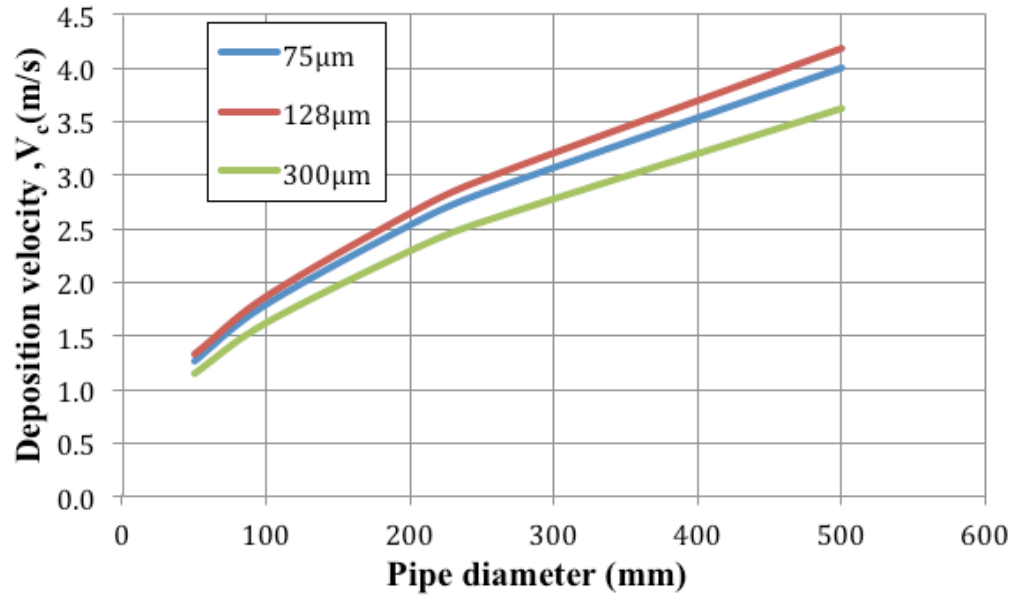
Figure 3.8 Predicted variation of deposition velocity with pipe diameter for a sulfur-liquid CO_2 slurry.

For the SEC analysis to provide the optimum particle size and solids concentration for liquid CO_2 slurries (pet coke and sulfur) in the hypothetical slurry pipeline, a suitable pipe size must be selected. The selection of the pipe size in this analysis is based on two criteria. First, mass or volumetric rate of the gaseous CO_2 captured and compressed to liquid CO_2 from the upgrading process is anticipated. Second, the flow velocity of liquid CO_2 (calculated from the anticipated mass or volumetric rate) in the chosen pipe size should be greater than the deposition velocity of the slurry in that pipe size. A recent report (**ICO$_2$N, 2011**) notes that two leading oil sands companies are planning to capture and sequester 1-1.2 million tonnes of CO_2 per year from their bitumen upgraders. Keeping in mind the rapid expansion of the oil sands industry, it would be safe to anticipate the mass rate of CO_2 capture from the upgrader of a given oil sands

43

company to rise to 2 million tonnes per year in the near future. A report from **Shell Canada Limited (2010)** on their CCS project assumes a negligible loss of 0.1% during the compression of the captured CO_2 in the upgrader. Therefore in our analysis, 2 million tonnes of liquid CO_2 per year can be assumed to be available for the hypothetical liquid CO_2 slurry pipeline. In that case, a 200mm pipe (8'') would be suitable because the mass rate of 2 million tonnes of liquid CO_2 per year in this pipe size would translate to a linear flow velocity of about 2.3m/s (see calculations, Appendix F). This velocity is greater than the deposition velocity of 2.1 m/s for 100-150μm pet coke particles in a 200mm pipe, as estimated using the SRC model. From a SEC point of view, a pipe size of 200mm is suitable because this diameter falls on the flat portion of the SEC vs. diameter curve, as demonstrated in Figure 2.1. The justification for using a narrow particle size range of 100-150μm for sizing of the hypothetical pet coke-liquid CO_2 pipeline is presented in the subsequent discussions. Before proceeding further, it should be mentioned here that for transporting 100-150μm sulfur particles with liquid CO_2 (same design mass rate), the pipe size would have to be slightly smaller than 200mm as the deposition velocity of the sulfur slurry would be slightly higher than it is for pet coke. For this SEC analysis for sulfur-liquid CO_2 slurries, a constant pipe diameter of 200mm is assumed, given the various uncertainties in liquid CO_2 flow rates and actual commodities to be transported.

The predicted variation of SEC with average particle size is illustrated in Figure 3.9, for a pet coke-liquid CO_2 slurry in a 200mm pipe at $V=1.1V_c$ and for C_{vd}=0.15, 0.30 and 0.35.
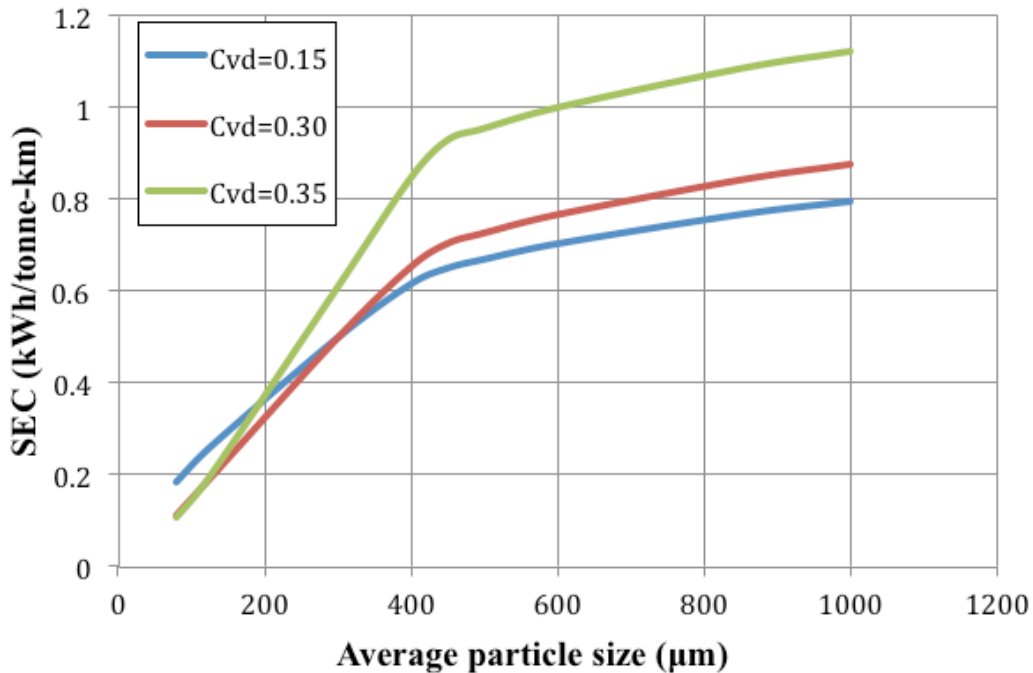
Figure 3.9 Predicted variation of SEC with average particle size for a pet coke-liquid CO_2 slurry: D= 200mm and $V=1.1V_c$.

It can be seen that for any given solids concentration, SEC increases with average particle size and this can be attributed to the direct proportionality of both friction components to particle size. However, particle size is more influential on the Coulombic friction component. In Figure 3.9, SEC appears to increase less steeply above particle sizes of 400µm. Beyond a certain particle size, deposition velocity no longer changes with increasing particle size. Hence, SEC for larger particles is calculated at lower velocities than that for lower particle sizes, thereby reducing the slope of the SEC curve at larger particle sizes. It is clear from Figure

3.9 that average particle sizes in the range of 100-150μm are the most economical for transportation of pet coke-liquid CO_2 slurry in 200mm pipe for any given solids concentration. Transporting particles much finer than 100μm will result in lower separation efficiency at the end point of the hypothetical liquid CO_2 slurry pipeline, assuming a hydrocyclone separator is used (**Park, 2003**). The lower separation efficiency from the liquid CO_2 stream means that some fraction of the particles is unavailable (lost) for subsequent transport to market by rail. In addition to the lower separation issue with finer particles, grinding energy required to produce particles smaller than 100μm rises exponentially (**Bremer, 2008**).

To select the optimum solids concentration of pet coke in the hypothetical 200mm liquid CO_2 slurry pipeline, two test cases are evaluated to show the effect of average particle size on SEC for a range of solids concentrations. This evaluation is illustrated in Figure 3.10, where predicted SEC is plotted against C_{vd} for 128μm and 300μm pet coke-liquid CO_2 slurries in a 200 mm pipe at $V=1.1V_c$.
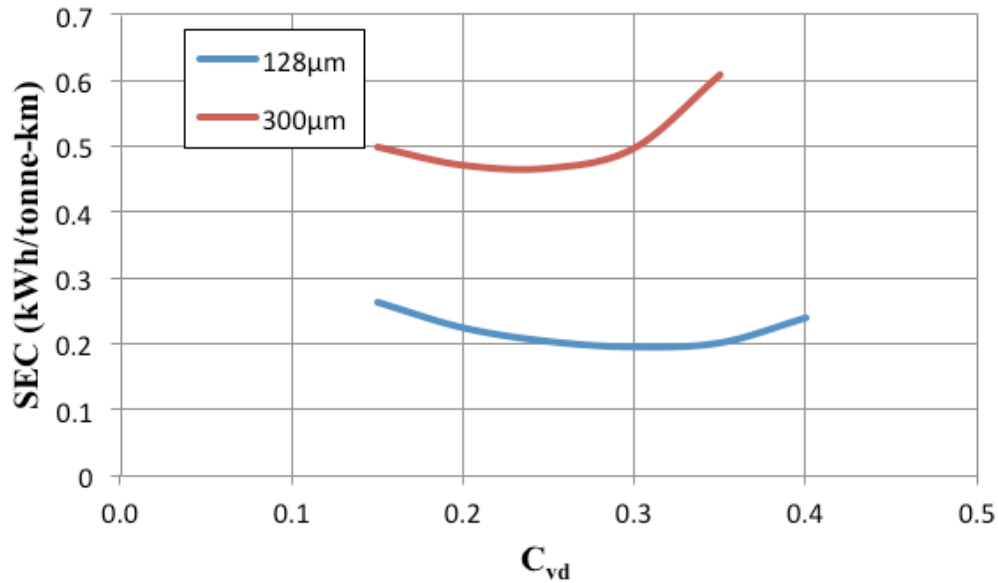
Figure 3.10 Predicted variation of SEC with C_{vd} for a pet coke-liquid CO_2 slurry: D= 200mm and V=1.1V_c.

From Figure 3.10, it is evident that for both particle sizes of pet coke in liquid CO_2, a minimum SEC is obtained. This trend shows that for a given flow velocity, it is not economical to transport the slurries at low concentrations, as the solids throughput is low. Also, employing very high concentrations is not economical either as those throughputs are achieved at the cost of very large hydraulic gradients. Hence, a minimum SEC is reached at an optimum delivered solids concentration for either particle size. It is worth noting here that, in Figure 3.10, the SEC minimum for either particle size would shift to a higher delivered solids concentration if the flow velocity is increased. In Figure 3.10, the SEC minimum for the 300μm slurry is reached at a lower solids concentration (C_{vd} =0.25) than that for the 128μm slurry (C_{vd} =0.30). This is due to the large hydraulic gradients

arising for the coarser particle slurry at higher concentrations, as seen in Figure 3.3. The upward shift of the SEC curve for the coarser particle slurry in Figure 3.10 can be attributed to its higher Coulombic friction.

Through analysis of Figures 2.2, 3.9 and 3.10, it can be said that the most energy efficient transportation of pet coke in liquid CO_2 in a 200mm pipe involves using an operating velocity of $V=1.1V_c$, particle sizes in the range of 100-150μm and delivered solids concentration of around 30% by volume.

Figure 3.11 shows the predicted variation of SEC with average solids particle size (d_{50c}) for a sulfur-liquid CO_2 slurry in a 200mm pipe at $V=1.1V_c$ and for $C_{vd}=0.15$, 0.30 and 0.35.
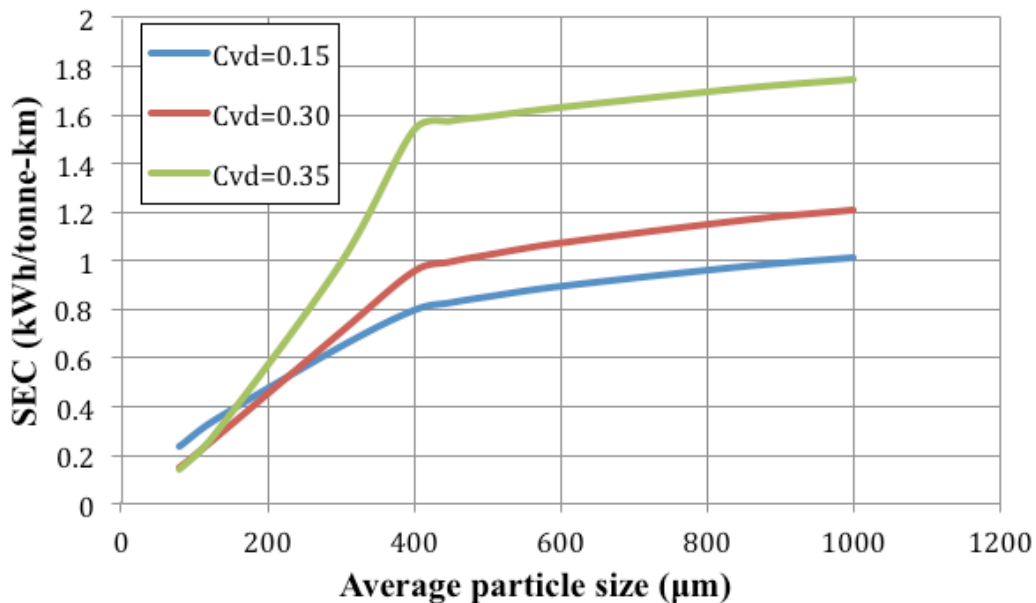
Figure 3.11 Predicted variation of SEC with average particle size for a sulfur-liquid CO_2 slurry: D= 200mm and $V=1.1V_c$.

It can be seen that trends observed here are similar to those seen in Figure 3.9. As expected, average particle size in the range of 100-150μm is the most economical for transportation of sulfur-liquid CO_2 slurry in a 200mm pipe for any given solids concentration. The optimum velocity for this particle size range remains the same, i.e., $V=1.1V_c$.

To select the optimum solids concentration of sulfur for the 200mm liquid CO_2 slurry pipeline, two test cases are evaluated again to show the effect of average particle size on SEC for a range of solids concentrations. This evaluation is illustrated in Figure 3.12, where predicted SEC is plotted against C_{vd} for 128μm and 300μm sulfur-liquid CO_2 slurries in a 200 mm pipe at $V=1.1V_c$.
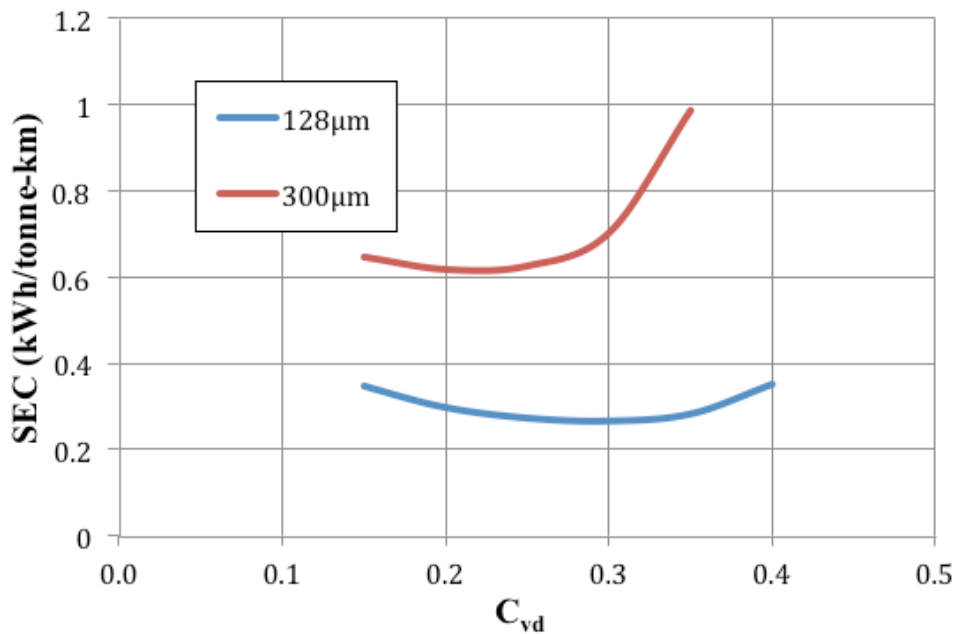
Figure 3.12 Predicted variation of SEC with C_{vd} for a sulfur-liquid CO_2 slurry: D= 200mm and $V=1.1V_c$.

It can be seen that the optimum concentration for the 128μm sulfur-liquid CO_2 slurry is around 30%, which is the same as that for 128μm pet coke-liquid CO_2

49

slurry, seen in Figure 3.10. However, the optimum solids concentration for the 300μm sulfur-liquid CO_2 slurry is C_{vd}=0.20, while the optimum solids concentration for the 300μm pet coke-liquid CO_2 slurry is C_{vd}=0.25. This is expected because sulfur has a higher density than pet coke, due to which a slurry of these components would have higher friction losses at higher concentrations for the coarser particles (see Figures 3.3 and 3.4). Hence, the minimum SEC for 300μm sulfur-liquid CO_2 slurry should occur at a lower solids concentration than that for a 300μm pet coke-liquid CO_2 slurry, with other operating conditions being the same.

The accuracy of the SEC calculations done for liquid CO_2 slurries in this study depends on the accuracy of the hydraulic gradient predictions obtained from the model. However, the performance of this model has not yet been tested for slurries like liquid CO_2 slurries, where the carrier fluid viscosity is very low. Hence, an experimental program is undertaken in this study to measure friction losses for slurries with low carrier fluid viscosities in a 50mm pipe loop and test the performance of the model. For the test program described here, hot water (70^0C) is used instead of liquid CO_2. The operating conditions (particle size and solids concentration) chosen for the 50mm pipe flow tests represent the optimum SEC conditions for transporting pet coke-liquid CO_2 slurries in the hypothetical 200mm pipe.

Figure 3.13 shows the variation of predicted SEC with C_{vd} for pet coke-liquid CO_2 slurry and pet coke-hot water slurry in a 50mm pipe with d_{50c}=128μm and at V=1.1V_c=1.15m/s for the pet coke-liquid CO_2 slurry and V=1.1V_c=0.88m/s for the pet coke-hot water slurry.
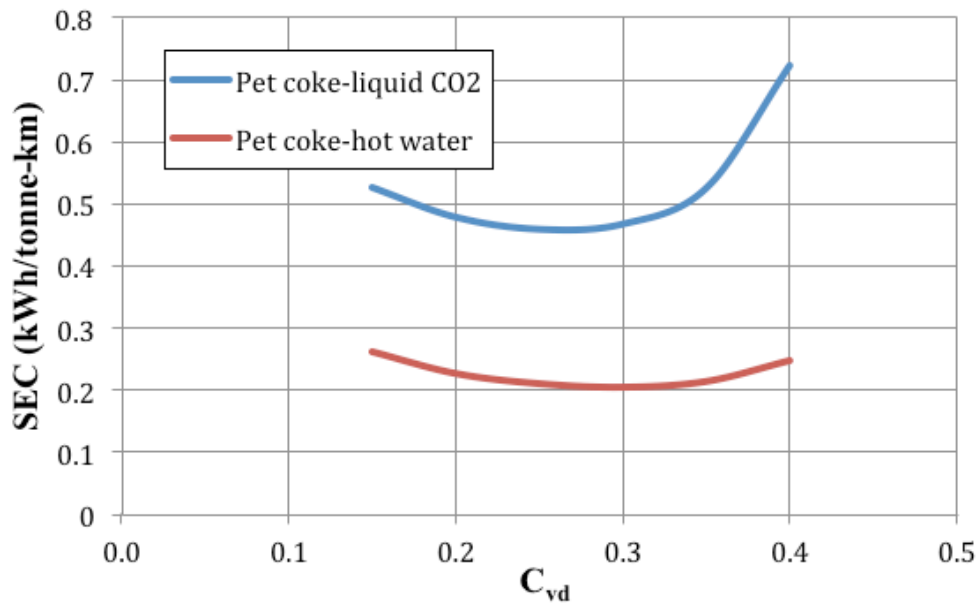
Figure 3.13 Predicted variation of SEC with C_{vd} for pet coke-liquid CO_2 slurry and pet coke-hot water slurry: D=50mm; d_{50c}=128μm; V=1.1V_c=1.15m/s for pet coke-liquid CO_2 slurry and V=1.1V_c=0.88m/s for pet coke-hot water slurry.

As seen from Figure 3.13, the SEC values for the pet coke-liquid CO_2 slurry are higher than for the pet coke-hot water slurry. This can be attributed to the slightly higher deposition velocity for pet coke in liquid CO_2, due to its lower viscosity. This results in SEC values for pet coke-liquid CO_2 slurry being calculated at a slightly higher velocity than that for the pet coke-hot water slurry. Additionally, the Coulombic friction component is slightly higher for the pet coke-liquid CO_2

slurry at these low velocities because of the lower viscosity of the suspending liquid. Minimum values of SEC are reached at C_{vd}=0.25 and 0.30 for pet coke-liquid slurry and pet coke-hot water slurry, respectively.

The range of solids concentrations tested in the loop for the 128μm pet coke-hot water slurry tests covers the optimum solids concentration for the pet coke-liquid CO_2 slurry in a 200mm pipe (C_{vd}=0.30 from Figure 3.10), the pet coke-liquid CO_2 slurry in a 50mm pipe (C_{vd}=0.25 from Figure 3.13) and the pet coke-hot water slurry in a 50mm pipe (C_{vd}=0.30 from Figure 3.13).

4 Experimental Method

4.1 50mm pipeline loop description

Figure 4.1 shows the schematic of the 50mm horizontal pipe loop used to collect experimental friction loss data for water, sand-water and pet coke-water slurries. The major components of the pipe loop circuit are the feed tank, progressive cavity pump and the 50mm pipeline. The feed tank has a capacity of 92 litres and a conical bottom with a slope of 30^0 for easy discharge of the slurry from the tank into the pump suction. A progressive cavity pump (Moyno 2F090G1CDB3SAC) with a 7.46kW (10HP) motor was used to circulate the slurries in the test loop. The mixture velocity was adjusted by changing the motor speed using the Baldor variable frequency drive (VS1GV210-1B). The pump and its motor were purchased from Wajax Industrial Components, Calgary while the drive was purchased from Alberta Industrial Controls & Drives Inc, Edmonton. The pipe loop itself is made from Schedule 40 stainless steel (SS-304 L) pipe. The internal diameter of the pipe was measured to be 52.8mm using vernier calipers. The value of the internal diameter was obtained from the average of 5 measurements taken at different points on the circumference of an available pipe spool. Figure 4.2 shows a photograph of the test loop.
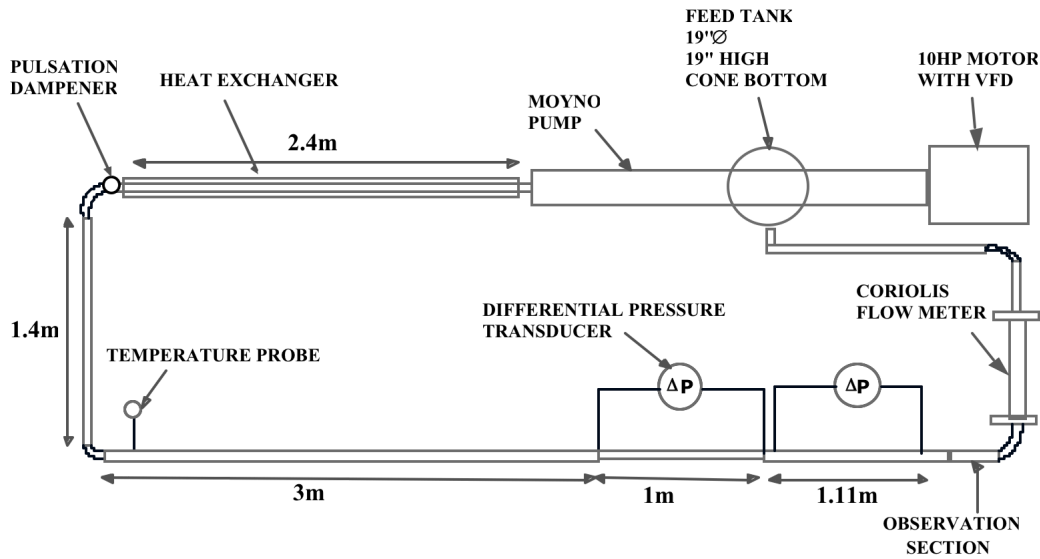
Figure 4.1 Schematic of the 50mm horizontal pipe loop used in the experimental program

The pipeline loop contained the following instrumentation: Coriolis flow meter (Micromotion F-series), differential pressure transducers (Rosemount 3051 series) and K-type thermocouple probe. The Coriolis flow meter was used to measure mass flow rate and density of the mixture and the differential pressure transducers were used to measure frictional pressure drop across the two test sections. Both the flow meter and differential pressure transducers were purchased from Spartan Controls Ltd, Edmonton. The K-type thermocouple probe (Omega) was used to measure mixture temperature, and it was supplied by the Instrument Shop, Department of Chemical and Materials Engineering, University of Alberta. The analog signals from the differential pressure transducer, flow meter and temperature probe were converted into digital signals in the central data

acquisition unit (NI cDAQ-9174). These outputs were then recorded and monitored in real time using LabVIEW.

Figure 4.2 Photograph of the 50mm horizontal pipe loop used in experimental program

Colwell and Shook (1988) experimentally determined the entry length for horizontal pipe flow of settling slurries to be of the order of 50 pipe diameters from tests with 190μm sand-water slurries in a 50mm loop. Hence, to ensure fully developed flow for the frictional pressure drop measurements in this loop, the first test section (1m long) was placed 3m (60 pipe diameters) from the upstream pipe elbow in the return leg of the pipe loop. A transparent section (0.3m long) was

placed downstream of the test sections to visually determine formation of a stationary deposit at the pipe bottom.

Domestic cold water was circulated in the annulus of the double pipe heat exchanger, which was 2.4m long with a 76mm (3'') ID shell, to absorb the heat arising from friction losses in the pipe and to maintain constant operating temperature. A pulsation dampener, which consisted of a vertical pipe 0.914m (3') long and 51mm (2'') in diameter, was installed in the outgoing leg of the loop. It was filled with air and isolated from atmosphere with a ball valve. It absorbed the flow pulses coming from the Moyno pump, thereby reducing vibrations in the pipe loop. An immersion heater (CXCT345P2), with capacity of 4.5kW, immersion length of 30cm (12") and equipped with a thermostat, was placed inside the mixing tank and was used to raise the water temperature for the pet coke-water tests conducted at 70^0C. The heater was purchased from CCI Thermal Technologies, Oakville, Ontario. The pipe loop was insulated to prevent heat loss and maintain constant temperature for the high temperature tests.

4.2   Pipe loop operation procedure

This section outlines the operating procedure used to obtain pipeline friction loss data (frictional pressure drop, flow velocity, and operating temperature) for water and slurry tests in the 50mm loop.

Before conducting the actual water or slurry tests at room temperature, the loop preparation step was implemented. In this step, the loop was filled with warm water (at 50^0C) and allowed to cool to room temperature overnight to reduce its

dissolved air content. The water level in the tank was kept at 1/4 of the tank height. The next day, the pump was started and its speed was increased slowly to circulate water at a velocity of 1 m/s in closed mode operation (flow returning to the pump suction). The sensing lines of the differential pressure transducer were opened and any remaining air bubbles in the loop were eliminated through the bleed valves on the differential pressure transducer. The pump was then switched off and the pressure transducer was "zero shifted" manually at no flow conditions.

For water tests at room temperature, following the loop preparation step, the pump was started again and set at a low velocity of about 0.6 m/s in closed mode operation. Pressure drop, temperature and mass flow rate were monitored using the LabVIEW program. When the readings became steady, the data were recorded for 2 minutes at 1 second intervals. Flow velocity was increased in steps until the maximum permissible velocity of 3.5m/s was reached. Data were recorded at each velocity. The pump speed was then gradually reduced for shut off. Zero readings of the transducers were verified after pump shut off, i.e. at no flow conditions.

For a given slurry test at room temperature, the loop preparation step was first completed and then the pump was started again in closed mode operation and its speed was set to produce a mixture velocity 10-15% higher than the predicted deposition velocity (estimated from the SRC two-layer model). Pre-weighed solids were slowly added in batches into the tank and fed into the pump suction at that set velocity, until the desired test solids concentration was prepared in the

loop. With the knowledge of carrier fluid density (ρ_f) and solids density (ρ_s), the mixture density (ρ_m) obtained from the Coriolis meter was used to verify the solids concentration prepared in the loop, using Equation 4.1. The discrepancy between the solids concentration determined from Equation 4.1 and that computed from solids addition into the tank was always small. The solids concentration determined from Equation 4.1 was used to determine the delivered solids concentration (C_{vd}) using Equation 4.2. In Equation 4.2, X_{44} is the fraction of the solids less than 44μm and is deduced from the particle size distribution of the solids. The delivered solids concentration (C_{vd}) of Equation 4.2 was further used as an input parameter in the SRC two-layer model.

$$C = \frac{\rho_m - \rho_f}{\rho_s - \rho_f} \qquad (4.1)$$

$$C_{vd} = C(1 - X_{44}) \qquad (4.2)$$

For a given delivered solids concentration and flow velocity, pressure drop and mass flow rate data were monitored with the LabVIEW program. When the readings became steady, the data were recorded for 2 minutes at 1 second intervals. Mixture density readings from the Coriolis meter were manually recorded at each velocity. Flow velocity was increased in steps until the maximum permissible velocity was reached. Data were recorded at each velocity. After testing a given delivered solids concentration over the entire velocity range, the flow velocity was reduced slowly to the initial starting velocity. More solids were then added into the tank and fed into the pump suction, until the next desired delivered solids concentration was reached. Data were recorded again in the

aforementioned fashion. At the end of the slurry runs, the flow velocity was set to 1.5 m/s and the drain valve was opened to collect the solids in the trough container (540 liter capacity, see Appendix E). Simultaneously, water was added into the tank from the supply line to flush the solids into the trough. Solids accumulated in the trough, while the water from the trough drained into a floor drain. After all the solids were removed (when the Coriolis meter indicated the density of only water), the drain valve was closed and the pump was switched off. Additional water test runs were performed after the slurry tests and the data from these water runs were checked with data obtained earlier to ensure data reliability.

For hot water or hot slurry tests, the loop was filled with 50^0C water and the level in the tank was kept high enough to ensure the return stream coming into the tank was submerged. Water was circulated in closed mode at a low velocity. Periodically (every 15 minutes), water was diverted into the tank, where the water was heated up from its circulation past the immersion heater. Once the water in the loop reached 70^0C, friction loss data were collected under closed loop operation at various increasing flow velocities, in the same fashion described for water runs conducted at room temperature. The flow velocity was then reduced for addition of the desired mass of pet coke and the slurry friction loss data were taken in the same fashion adopted for slurry tests at room temperature.

The pet coke used for the tests was "pre-conditioned" before it was added to the loop for the slurry flow tests. In this process, batches of pet coke were mixed with

59

water at 50^0C in large containers and were soaked for at least 24 hours before the tests were conducted. The pre-conditioning stage was necessary to remove light ends from the pet coke and also it was an attempt to reduce the concentration of air bubbles attached to the surface of the particles. The hydrophobic nature of the pet coke allowed tiny air bubbles to attach to the particle surface during loading of the slurry in the loop. These air bubbles would then be released and would cause errors in pressure transducer readings when they entered the sensing lines of the transducer. In spite of the pre-conditioning, air bubble accumulation in the sensing lines was still an issue during the high temperature runs. Therefore, the pressure test section of the loop was rotated by 90^0 to move the pressure taps, which were initially at the top of the pipe, to the horizontal plane. This helped to prevent air bubbles going into the sensing lines of the pressure transducer for pet coke-water runs at high temperature.

4.3   Materials

Three different sets of particles were used for conducting slurry flow tests: sand of two different sizes and petroleum coke. The sand was supplied by Lane Mountain Company, Valley, Washington, USA while Syncrude Canada Ltd provided the petroleum coke. The density of the Lane Mountain sand was taken as 2650 kg/m^3 (**Schaan, 2001**) and the density of petroleum coke was taken as 1600 kg/m^3 (**Gillies, 2012**). The particles were characterized by measuring their particle size distributions and settled bed concentrations. The methods for these tests are presented in the following section.

4.4   Laboratory tests

4.4.1   Particle size distribution

Particle size distributions were determined using the Malvern Mastersizer 2000. In this instrument particles passing through the laser beam cause the laser light to scatter. The angle and intensity of the scattered light is related to the size of the particles. The measurement procedure consists of three steps: the preparation of the dispersant in the test vessel, addition of the particles into the vessel for dispersion, and analysis of the dispersed sample by laser diffraction. In the first step, the test vessel was filled with the dispersant or de-ionized water, which continuously re-circulated between the vessel and the test window (window through which laser beam passes through the test sample). Water in the vessel was then stirred at maximum speed and the stirrer was switched off. In this process, air bubbles rose to the surface and were eliminated. The stirrer was started again and was kept switched on for the remaining test duration. Stirring was done to prevent particles from settling in the vessel during addition of the particles and analysis of the sample. Before adding the particles, a background measurement was performed to account for laser scattering due to any contaminants in the dispersant or any dust on the test window.

 In the second step, the container, half-filled with dry solids, was tilted and gently rolled sideways for about 20 seconds in an attempt to mix the solids and obtain a representative sample for size analysis. Solid particles were then taken out from the container with a spatula and were added to the vessel. The addition of solids

was continued until critical obscuration of the laser beam from the dispersed sample was achieved.

In the final step, the size measurement analysis was conducted. Detectors placed at fixed angles recorded the intensity of scattered light and particle size distribution was calculated from the recorded intensities. This method was preferred over dry sieve analysis for obtaining particle size distributions, as smaller quantities of sample are required and good measurement accuracy (less than 1% error) is typically attained. The particle size distributions of the solids obtained from the Malvern Mastersizer 2000 were further analyzed to determine the fraction of solids that are fines (X_{44}) and the coarse particle d_{50}.

4.4.2 Settled bed concentration (C_{max})

Settled bed concentration (C_{max}) represents the limiting concentration of the coarse particles in the slurry at which the distance between adjacent particles approaches zero and the slurry's resistance to flow approaches an infinite value. This is one of the important input parameters in the SRC two-layer model for obtaining friction loss predictions for settling slurries and therefore measurement of C_{max} is necessary for this study.

A batch settling test was used to determine the settled bed concentration of the particles. This method is quite well known (**Singh et al., 2001; Gillies, 2012**). In this method, a known mass of solids was placed in a 1000 ml graduated cylinder. Water was added to prepare a mixture with a solids concentration of 30% by

volume. The cylinder was capped using parafilm foil and the slurry was well mixed. The cylinder was left undisturbed for particles to settle until the settling was complete and the bed height could be determined. The settling time varies with particle type, but is typically in the order of 2 to 5 days. Once settling was complete, the cylinder was slightly lifted and gently tapped on the countertop to promote the formation of the settled bed. This process was continued until the volume of the settled bed did not change. The settled bed volume was then noted. The settled bed concentration was then calculated from the ratio of the known volume of the added particles to the measured volume of the settled bed.

4.4.3   Carrier fluid viscosity

The carrier fluid viscosity of selected slurry samples was measured using an ARG2 rheometer. The schematic of the concentric cylinder rheometer (**Gillies, 2012**), used for the measurements, is shown in Figure 4.3, where the spindle had a radius, R_1, of 14 mm and a length, L, of 42.03 mm. The cup had a radius, R_2, of 15.2 mm. A sample of slurry either taken from the 50mm loop or freshly prepared was sieved through the 325-mesh sieve. The slurry sample passing through a 325 mesh (44μm) sieve was tested in the rheometer. Using the measured values of the torque (T) collected at different spindle speeds (ω), T/L is plotted against ω to determine the carrier fluid viscosity (μ), as seen in the integrated equation for concentric cylinder viscometry of a Newtonian fluid (**Shook et al., 2002**):

$$\frac{T}{L} = \frac{4\pi\mu\omega}{\left[\frac{1}{R_1^2} - \frac{1}{R_2^2}\right]} \qquad\qquad (4.3)$$

For the samples, carrier fluid viscosities were measured in the temperature range

of 20 to 22^{0}C.
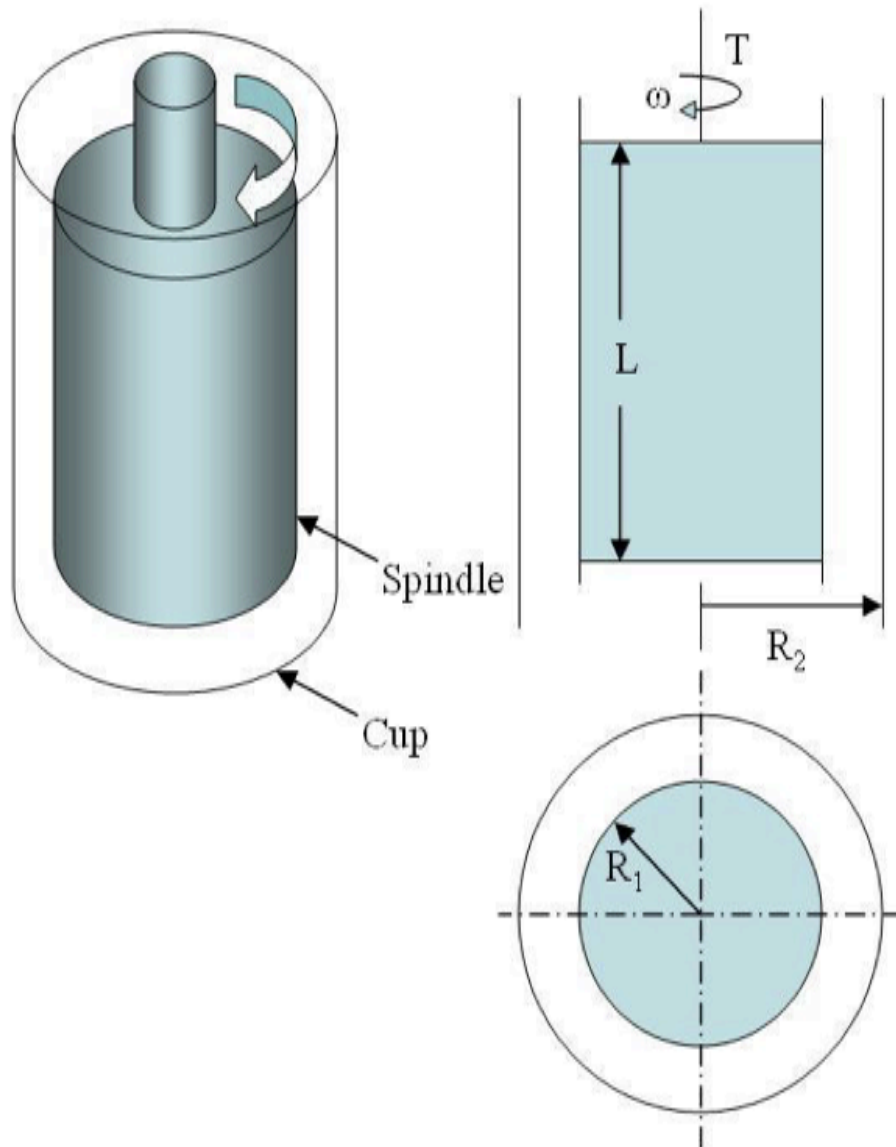
Figure 4.3 Schematic of the concentric cylinder rheometer used for carrier fluid viscosity measurements

5 Results and Discussion

5.1 Overview

This chapter describes the results gathered during this project in the following order: Results from the particle characterization tests, described in Section 4.4, are presented in Section 5.2. Data collected from the water runs at 25^0C and from all the slurry tests at 21^0C are analyzed and discussed in Section 5.3. Data collected from pet coke-water runs at 70^0C are analyzed and discussed in Section 5.4. Independent to the results discussed in Sections 5.2-5.4, a proposal for a simple measuring technique to measure coefficient of friction for any solid particle-pipe material combination is presented in Section 5.5. Table 5.1 shows the overall range of test conditions for all the tests performed with the 50mm loop.

Table 5.1 Overall test matrix for all the tests conducted in the 50mm loop

Test system	Temperature (^{0}C)	Deposition velocity, V_c (m/s)	Velocity range (m/s)	Test solids concentration range (v/v%)
Water	25	N/A	0.6-3.5	N/A
	70	N/A	1.8-4.9	N/A
96µm sand-water	21	1	1.4-3	5-15
174µm sand-water	21	1.4	1.5-3.2	15-30
	70	1.50	1.8-4	15-25
128µm pet coke-water	21	0.75	0.9-3.3	15-37
	70	0.90	2.1-4.9	15-35

5.2 Particle characterization

Particle size distributions of the particles used for the slurry tests, as measured with the Mastersizer 2000, are plotted in Figure 5.1. The data for these distributions can be found in tabular form in Appendix A. The volume-median diameter or d_{50} of the entire particle population, d_{50} of the coarse fraction (>44µm) and volume fraction of the particles less than 44µm (X_{44}) were obtained from the distributions and are presented in Table 5.2. The settled bed

66

concentrations (C_{max}) of these particles, determined using the method described in Section 4.4.2, are also reported in Table 5.2. The raw data for the C_{max} calculations can be found in Appendix A.
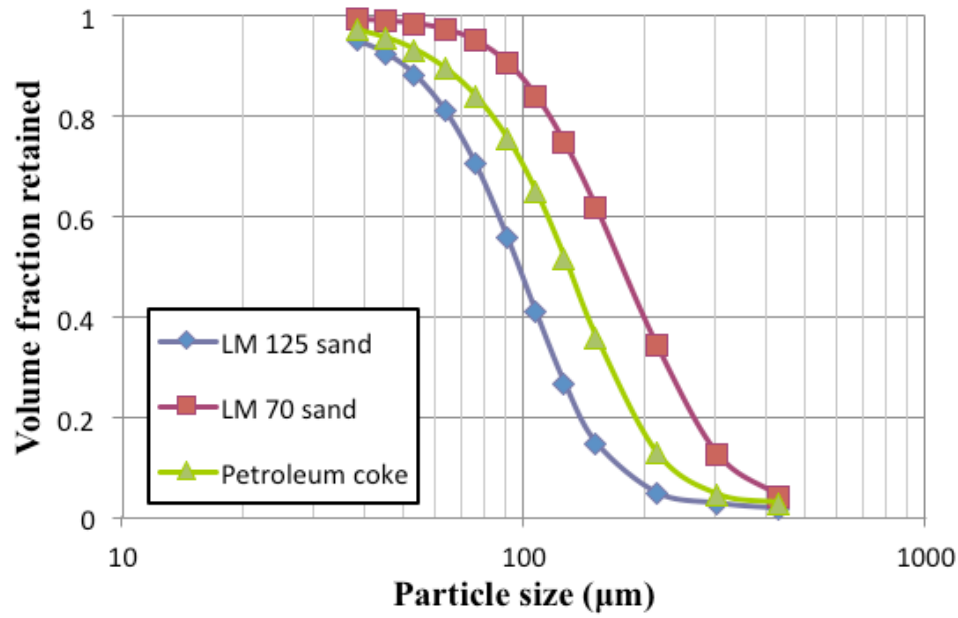
Figure 5.1 Particle size distributions of the particles used for slurry tests in 50mm pipe loop

Table 5.2 Properties of the particles used for pipe loop tests

Particles	d_{50} (µm)	Coarse fraction (+44µm) d_{50c} (µm)	X_{44}	C_{max}
LM 125 sand	96	100	0.0724	0.50
LM 70 sand	174	175	0.0068	0.516
Petroleum coke	128	131	0.0416	0.60

Fines content (<44µm) in LM 125 sand and petroleum coke were 7.24% and 4.16% by volume respectively, while in LM 70 sand the fines content was

67

negligible. Comparing the measured C_{max} values of LM 125 or LM 70 sand with petroleum coke, it can be inferred that Lane Mountain sand is more angular than the pet coke, since the latter has a higher C_{max} value. This is because settled bed concentration decreases or voidage increases as particle shape becomes less spherical or more angular. It can be seen further in Section 5.3.2 that particle sphericity also has an effect on pipeline friction losses. **Schaan (2001)** and **Gillies (2012)** had used LM 125 sand and petroleum coke respectively for their slurry tests. **Schaan (2001)** measured the C_{max} of LM 125 sand and found it to be 0.505 and **Gillies'(2012)** measurement of C_{max} for pet coke provided a value of 0.61. Their values are in very good agreement with the measured C_{max} values obtained for the present study and reported in Table 5.2.

5.3   Pipe loop validation tests

5.3.1   Water tests at room temperature

A series of single-phase (water alone) flow tests at room temperature (25^0C) was conducted to commission the loop and determine the pipe's hydraulic roughness, which is used as one of the input parameters to obtain friction loss predictions for slurries using the SRC two-layer model. For a range of water velocities, the frictional pressure drop was measured across two test sections (Test Section 1 and Test Section 2, respectively, 1.0m and 1.11m long) in the return leg of the loop (see Figure 4.1). The pressure gradient data, i.e., pressure drop divided by test section length, were then used to determine the hydraulic roughness of the test pipe. For Test Section 1 (TS1), Figure 5.2 shows the experimental pressure gradients for water as a function of velocity. Also shown on the figure are the

68

predicted pressure gradients from the Churchill correlation (**1977**) for 50mm pipe. It can be seen in Figure 5.2 that when assuming the hydrodynamic roughness to be 10μm in the Churchill correlation, the experimental pressure gradient for water agreed well with the predicted values over the entire operating velocity range. For all further data analysis, the pipe roughness was taken as 10μm. All the friction loss data can be found in tabular form in Appendix B.
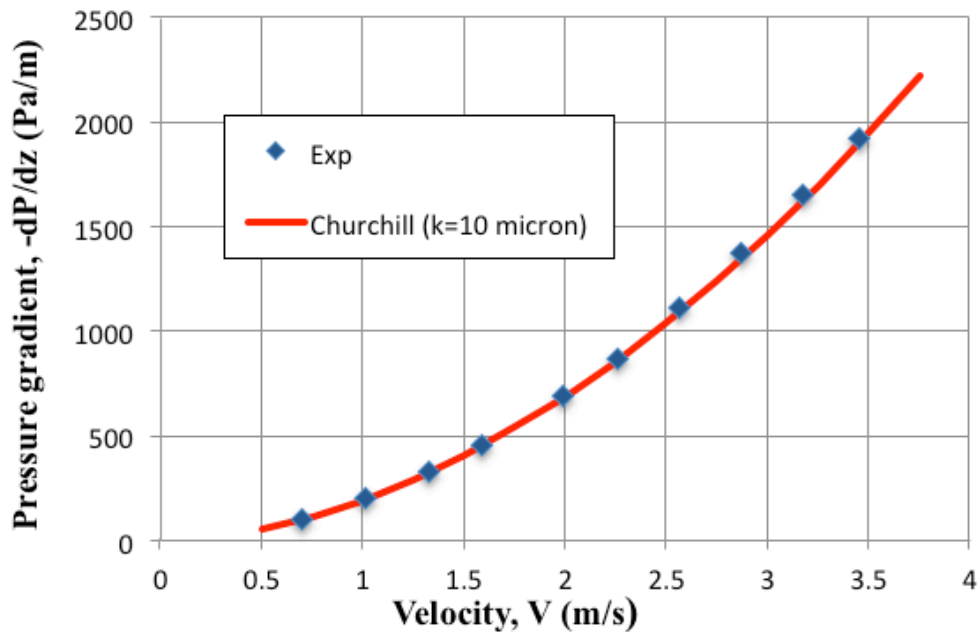
Figure 5.2 Comparison of pressure gradients obtained for water (from Test Section 1) with predicted pressure gradients from Churchill correlation: D=50mm;T=25^{0}C

Figure 5.3 shows the experimental pressure gradient for water as function of velocity for Test Section 2 (TS2). The downstream tap of TS2 was 0.48m from the elbow. For the same velocity, pressure gradients in TS2 were higher than those measured for TS1 and the discrepancy in the pressure gradients between the two test sections increased with increasing velocity. Theoretically, in the fully

developed flow region, the pressure gradient should be the same in both test sections. Here, it is suspected that that the elbow downstream of TS2 creates a flow disturbance and this disturbance propagates upstream to affect TS2 i.e., causes the pressure gradient in this section to increase.
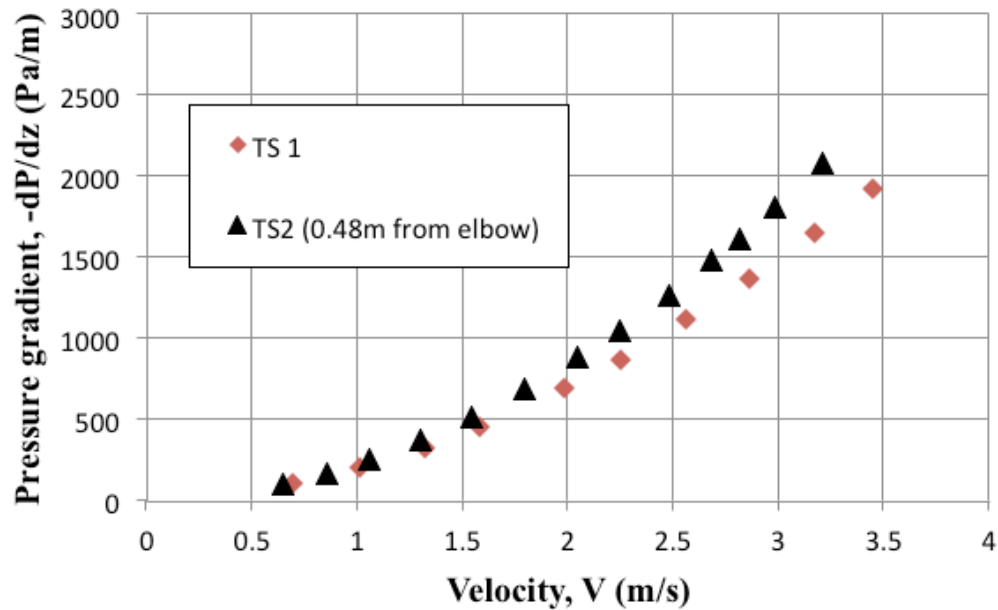
Figure 5.3 Comparison of experimental water pressure gradients as obtained from the two test sections TS1 and TS2: D=50mm; T=25^{0}C

To confirm our suspicions regarding the flow disturbance in Test Section 2, the downstream sensing line of Test Section 2 was shifted to a new tap closer to the elbow and pressure gradients were measured again for a range of velocities. Figure 5.4 shows the result from these downstream measurements. The measured pressure gradients for TS2 increased further on shifting the tap closer to the elbow. Again, the discrepancy in the pressure gradients increased with increasing velocity. The results shown in Figure 5.4 confirm the flow disturbance (end effects) assertion for TS2. Therefore, pressure gradient measurements from this

70

test section cannot be trusted to be representative of fully-developed pipe flow conditions. Therefore, in the subsequent discussion, only pressure gradient data from TS1 are analyzed.
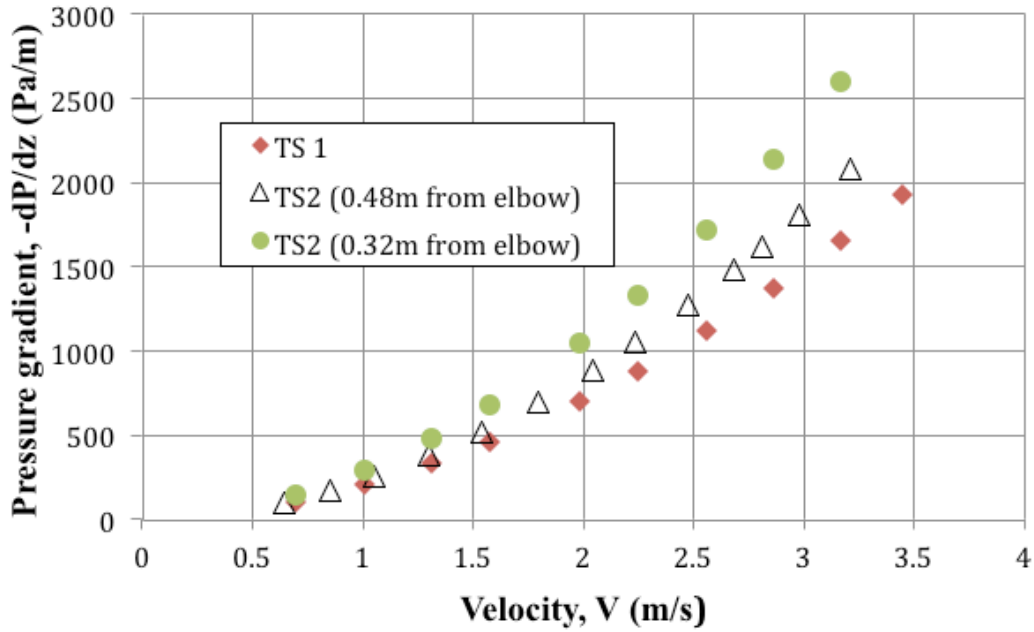
Figure 5.4 Comparison of water pressure gradients measured for TS2, using two different locations of the downstream pressure tap

5.3.2   Slurry tests at 21^0C

Slurry tests were conducted at 21^0C with the two Lane Mountain sands and the petroleum coke using the 50mm loop. The pressure gradient data obtained from the slurry tests were converted to hydraulic gradients using Equation 2.2. These hydraulic gradients were compared either with the values taken from the literature or with the predictions obtained using the SRC two-layer model (Pipe Flow 10) to confirm that good quality slurry friction loss data were produced using this loop. All slurry tests were conducted above the deposition velocity, V_c, estimated from the SRC two-layer model and these deposition velocities are included in Table 5.1. For all particles in this study, V_c was estimated on the basis of their coarse

d_{50}, except for pet coke, whose V_c was estimated on the basis of its coarse d_{85}. This was done to ensure largest pet coke particle would not settle, as it has a relatively broad size distribution. The data (pressure gradient, mixture velocity, mixture density from Coriolis meter) for all the slurry tests can be found in Appendix B. Before the slurry flow data sets are discussed, it should be noted here that the value of delivered solids concentration from the Coriolis meter (computed from Equation 4.2) increased slightly from the initial concentration prepared in the loop with increasing flow velocity. For a given test run, the average of these concentrations at all tested velocities is reported in that data set.

Figure 5.5 shows the measured hydraulic gradient as a function of mixture velocity for the 96μm sand-water slurry at 21^0C for three mixture concentrations. The measured hydraulic gradient for water alone is shown for comparison. For the 96μm sand slurry, the difference in hydraulic gradient between the slurry and the water increased as the velocity increased, which is a characteristic feature of fine particle slurries with dominant kinematic friction (**Schaan, 2001**). The increase in hydraulic gradient for the slurry with increasing solids concentration was attributed to increase in inter-particle dispersive stress with increasing concentrations.
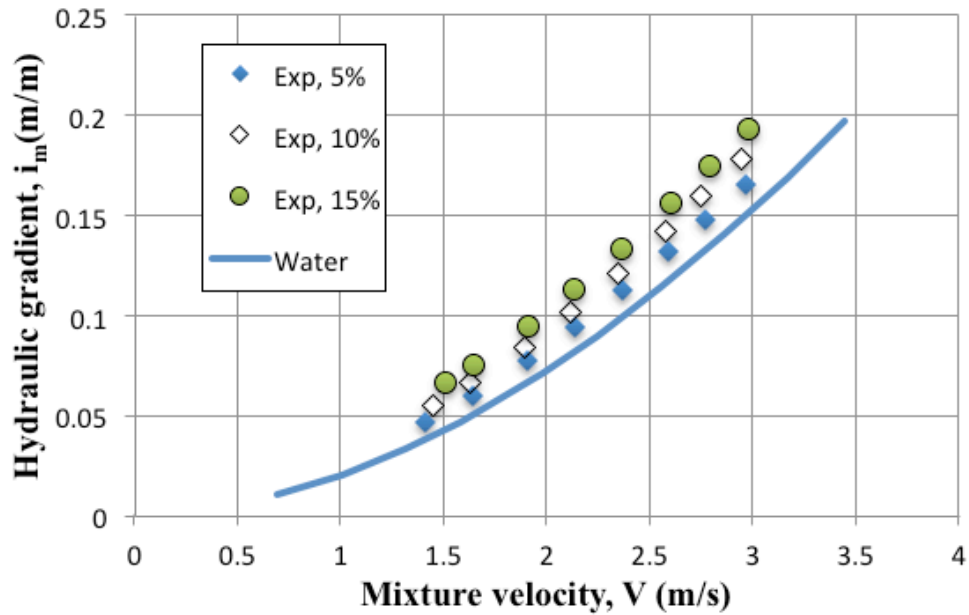
Figure 5.5 Variation of Experimental hydraulic gradient with mixture velocity for sand-water slurry: D=50mm;d_{50c}=100µm; T= 21^{0}C

Figure 5.6 shows the comparison of the measured hydraulic gradient values for 96µm sand-water slurry with the data obtained by **Schaan (2001)** and with the SRC model predictions. The input parameters for the SRC model with their values for all the slurry tests are given in Appendix D. In Schaan's work, one of the data sets was obtained using 90µm Lane mountain sand in a 50 mm loop at a solids concentration of 15% by volume at 15^{0}C. It can be seen that our data is in reasonable agreement with both Schaan's data set and SRC model predictions, with an average error of 9.54% and 11% from Schaan's data set and SRC model predictions respectively.
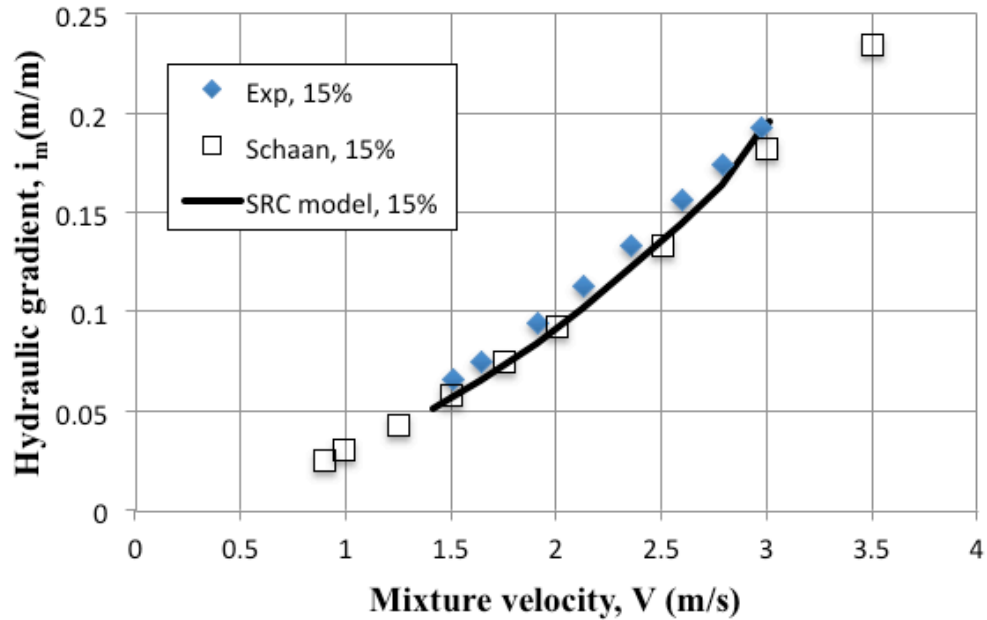
Figure 5.6 Comparison of the experimental hydraulic gradient values with Schaan's (2001) data set and SRC's model prediction for sand-water slurry: D=50mm;d_{50c}=100µm; C_{vd}=0.15 ;T= 21^{0}C

Figure 5.7 shows the measured hydraulic gradient as a function of mixture velocity for 174µm sand-water slurries at 21^{0}C for three test concentrations, along with the measured hydraulic gradient for water alone. As compared with the 96µm sand-water slurry, there is considerable Coulombic friction at lower velocities (< 2m/s) and this is evident in the upward shifting of the friction loss curves with respect to the water curve for successively increasing concentrations. The increasingly non-linear friction loss behaviour of the slurry at high concentrations (30% by volume) and at higher velocities is due to emergence of high inter-particle dispersive stresses (**Gillies and Shook, 2000)**.
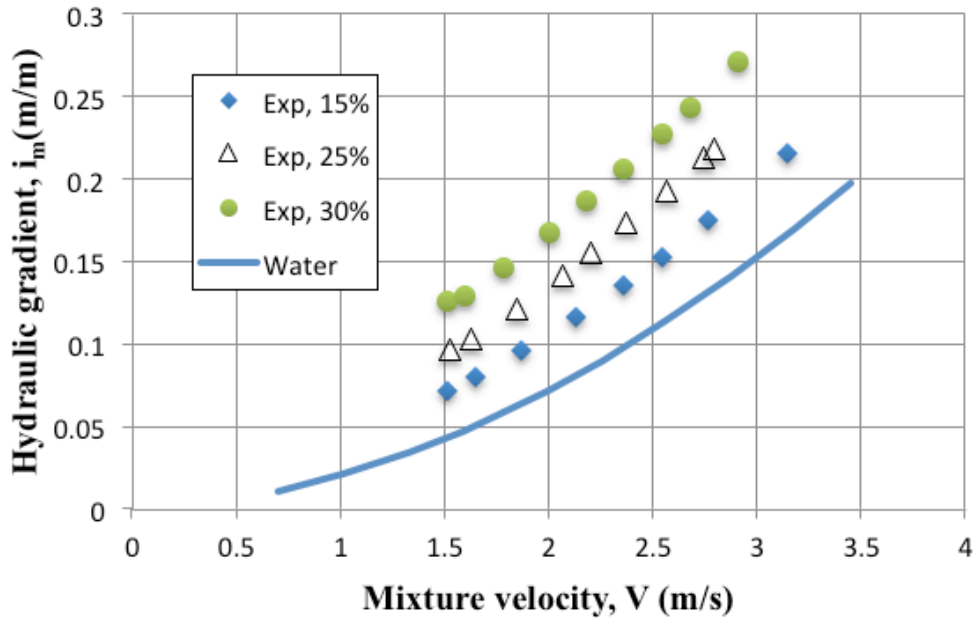
Figure 5.7 Variation of Experimental hydraulic gradient with mixture velocity for sand-water slurry: D=50mm;d$_{50c}$=175µm; T= 21^{0}C

Figure 5.8 shows the comparison of the measured hydraulic gradient values for the 174µm sand-water slurry with those obtained by **Gillies (1993)**. In his experiments, two of his data sets were obtained using 180µm sand in a 50 mm loop for solids concentrations of 15% and 30% by volume at 15^{0}C. It can be seen that for 15% solids concentration, the present data set is in good agreement with that obtained by **Gillies (1993)** with an average error of 5.1%. However, for 30% solids concentration, the present hydraulic gradients are much higher than that obtained by **Gillies (1993)**. This difference was expected as his experiments were done with a more rounded (less angular) sand and **Schaan et al. (2000)** had observed that pipeline friction losses increase with increasing particle angularity at higher concentrations. It can also be said that SEC increases with increasing particle angularity, when other operating conditions stay the same.
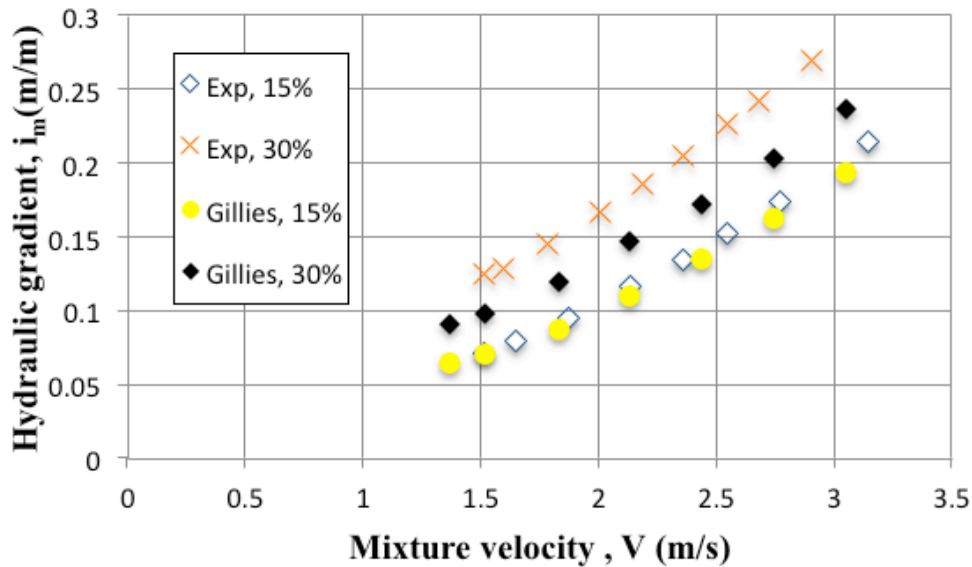
Figure 5.8 Comparison of the experimental hydraulic gradient values with the Gillies'(1993) data sets for sand-water slurry: D=50mm;d_{50c}=175µm; C_{vd}=0.15 and 0.30;T= 21^0C

Figure 5.9 shows the comparison of the measured hydraulic gradients of the present study for the 174µm sand-water slurry with the SRC model predictions. It should be noted that, as the fines content for this sand was almost negligible, the carrier fluid viscosity was not measured and the viscosity of water at 21^0C was used as the input in the model. The density input in the model accounted for the negligible fines. The measured data agree reasonably well with the model predictions, except for the 30% data at lower velocities. Lower friction losses for the 30% data at lower velocities is suspected to be due to possible particle degradation in the loop, thereby reducing both the concentration of coarser particles and the Coulombic friction at lower velocities. Particle degradation

would have possibly happened due to continuous re-circulation and flow velocity swings of the slurry for a reasonably long time (nearly 4 hours) till the attainment of higher concentrations. The average errors in the data sets from the model predictions were 4.1%, 5.4% and 7.56% for 15%, 25% and 30% solids concentrations respectively. The good agreement between the previous two data sets (96μm and 174μm sand-water slurries) and the model predictions is not surprising since the correlations used in the model were primarily developed from a database of sand-water slurry tests at room temperature conducted with various particle and pipe sizes.
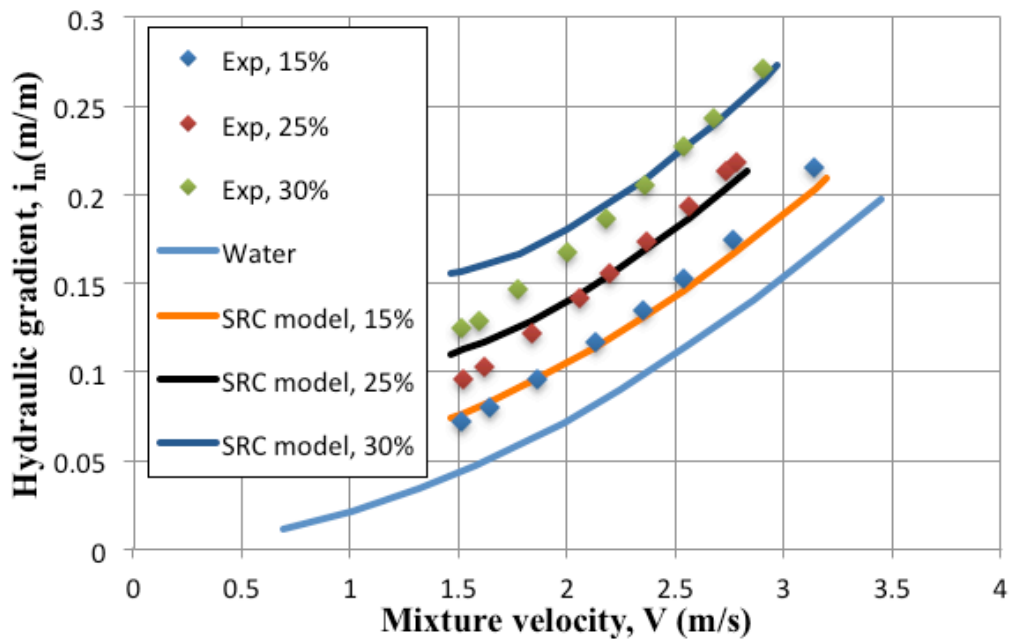
Figure 5.9 Comparison of the experimental hydraulic gradient values with the predicted values for sand-water slurry: D=50mm; d_{50c}=175μm; T= 21^{0}C

Based on the observations made from Figures 5.5-5.9, it is clear that the present set-up is capable of producing reliable hydraulic gradient data for coarse particle slurries. It is worth noting that the hydraulic gradient data from **Schaan (2001)**

and **Gillies (1993)** were obtained in fully developed flow conditions, with entry lengths in their 50mm loops being 60D and 120D respectively. Hence, Figures 5.6 and 5.8 demonstrate that the entry length chosen in the return leg of the test loop (60D) was adequate to obtain fully developed flow conditions for coarse particle slurries at room temperature. For slurry tests at higher temperature (70^0C), the chosen entry length was taken in confidence because entry length has been shown to decrease with increase in settling behavior of slurries **(Colwell and Shook, 1988)** and such behavior can be expected with increasing temperature or a reduction of carrier fluid viscosity.

Figure 5.10 shows the measured hydraulic gradients as a function of mixture velocity for the 128μm pet coke-water slurry at 21^0C for three different test concentrations. The measured hydraulic gradient for water alone is shown for comparison. It is clear from Figure 5.10 that, generally, the trends observed here were the same as those for the 174μm sand-water slurry tests conducted at room temperature. For similar solids concentrations and at lower flow velocities, the Coulombic friction was higher for the 174μm sand-water as compared with this slurry. For similar solids concentration and at higher velocities, the inter-particle dispersive stress in the pet coke-water slurry was lower as compared with the 174μm sand-water slurry due to the lower density of pet coke. This can be understood from the particle kinematic friction modeling in the SRC model (Equation 2.17), where the particle dispersive stress (τ_s) is directly proportional to the solids density.
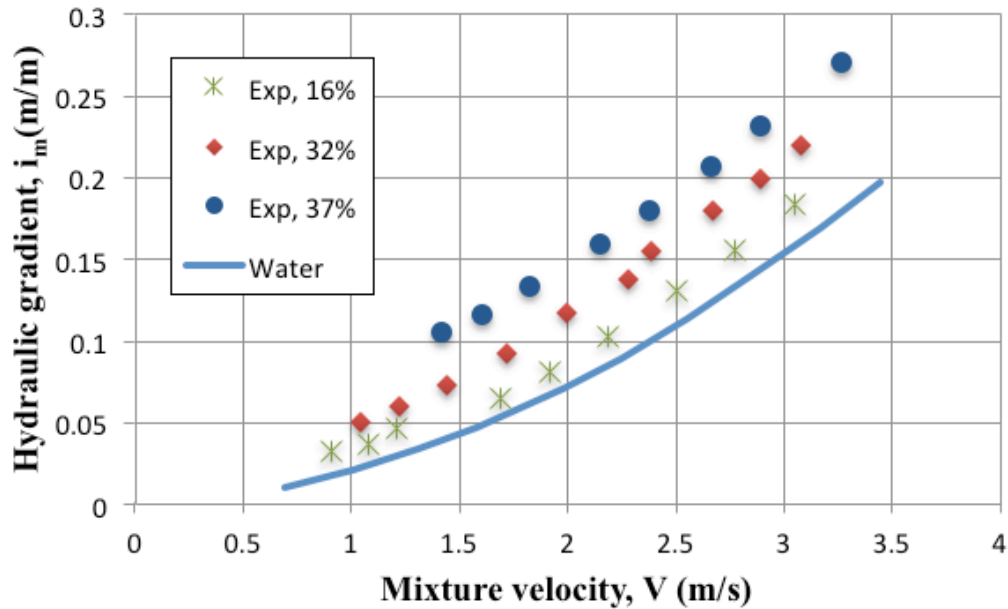
Figure 5.10 Variation of Experimental hydraulic gradient with mixture velocity for pet coke-water slurry: D=50mm; d_{50c}=131µm; T= 21^{0}C

Figure 5.11 shows the comparison of the measured hydraulic gradient values for the 128µm pet coke-water slurry with the SRC model predictions for 16% solids. To account for the effect of the pet coke fines content on carrier fluid viscosity, a 16% pet coke sample was prepared and sieved through a 325-mesh sieve. The underflow of the sample was tested in a rheometer and the measured viscosity was used as the input in the model. It can be seen from Fig 5.11 that the model predictions are very good for velocities higher than 1.5 m/s, with the average error from the predictions being 5.87%. For velocities around 1 m/s, experimental hydraulic gradients were very high with average error from the predictions being 42.3%. It is suspected that, at these low velocities, being close to the estimated V_c (0.73 m/s), a stationary bed would have started to form, thereby increasing the friction losses. This observation is reasonable, as one can expect a certain degree

of error in the V_c estimation from the model. Although model predictions for 32% and 37% solids concentrations of pet coke-water runs are not discussed here, it is expected that model predictions will be good for these concentrations at the higher end of the tested operating velocity range. Model predictions for 32% and 37% solids concentrations of pet coke-water runs are not shown here as carrier fluid viscosities of samples for these concentrations could not be measured in due time.
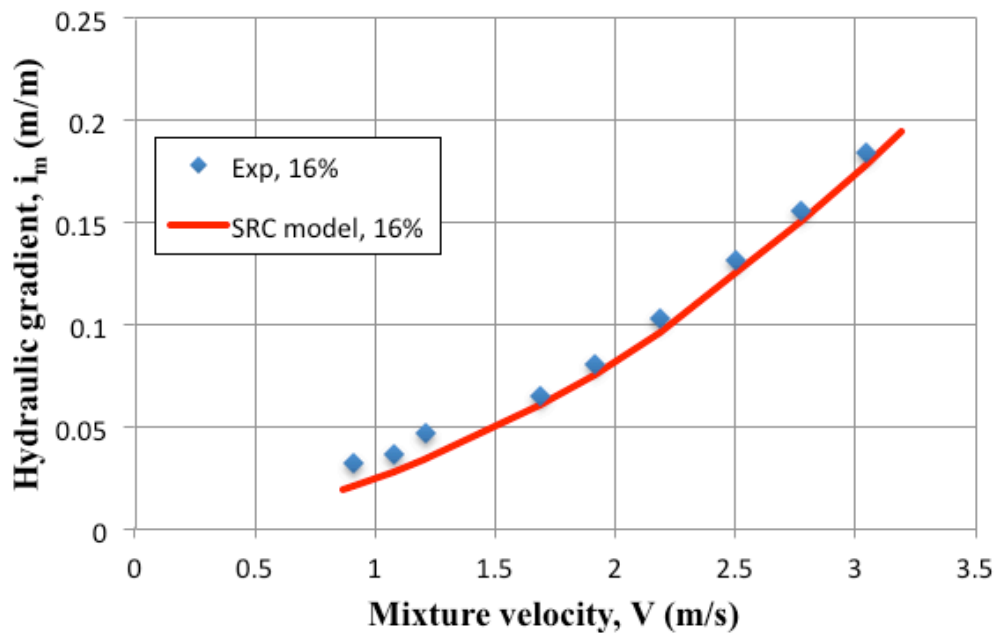
Figure 5.11 Comparison of the experimental hydraulic gradient values with the predicted values for pet coke-water slurry: D=50mm;d$_{50c}$=131μm; C$_{vd}$=0.16;T= 21^{0}C

Generally, the data collected from the slurry tests at room temperature with two sand particle sizes and pet coke were reasonable. Data for the 96μm sand-water slurry matches reasonably well with the literature and with the SRC model. The same can be said for the 174μm sand-water slurry, except for the data points at higher concentrations and at lower velocities. The pet coke slurry data (16% by

volume) was in reasonable agreement with the SRC model, except for the lower velocities when the formation of a stationary bed was suspected.

5.4   Pet coke slurry tests at 70^{0}C

In this section, results from pet coke-water tests at 70^{0}C are presented. It should be noted here that the range of solids concentrations tested for the pet coke-hot water slurries in the 50mm pipe loop covers the optimum or most economical solids concentration for transportation of pet coke liquid CO_2 slurry in the hypothetical 200mm pipeline, as shown in the calculations of Chapter 3.

Figure 5.12 shows the measured hydraulic gradient as a function of mixture velocity for 128μm pet coke-water slurry at 70^{0}C at four different test concentrations, along with the measured hydraulic gradient for hot water alone. The minimum test velocity was much higher than the estimated deposition velocity of 0.90 m/s. The hydraulic gradient data draw out a shape similar to that of the 96μm sand slurry at 21^{0}C. This also indicates that the kinematic friction is dominant in pet coke slurries at high temperature. Therefore, the pet coke-hot water friction loss data were used to determine if the f_s correlation in the model could predict the kinematic friction component for slurries with low carrier fluid viscosities.
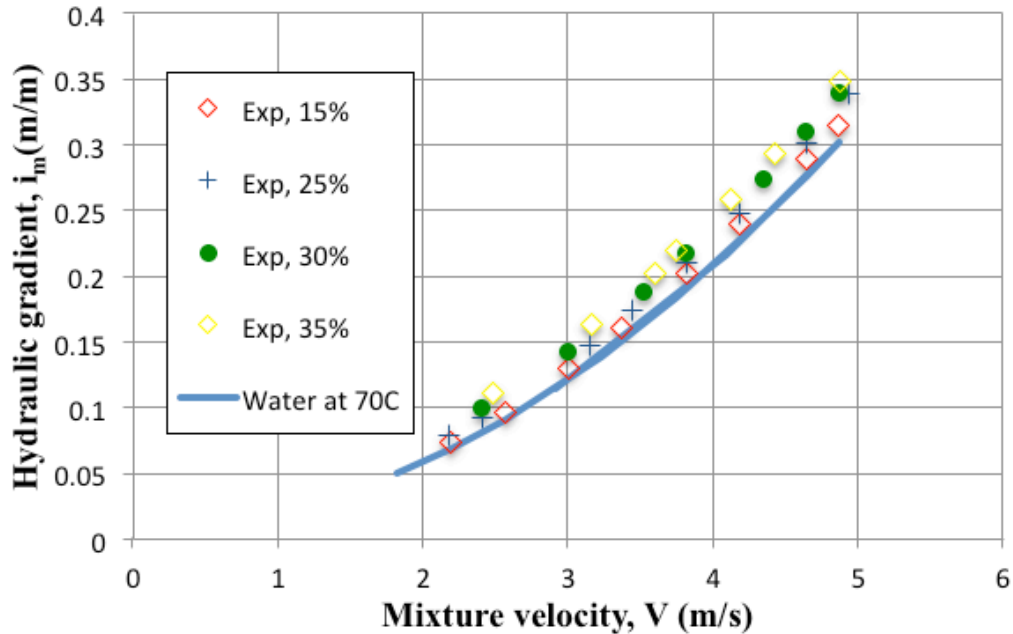
Figure 5.12 Variation of Experimental hydraulic gradient with mixture velocity for pet coke-water slurry: D=50mm; d_{50c}=131µm; T= 70^0C

The friction loss data were used to calculate the experimental solids friction factors using Equation 2.17. These values were then compared with f_s values from the model (Equation 2.18). The following steps were followed in calculating the solids friction factors from the experimental data:

1. **Wilson's (1976)** expression for threshold turbulent velocity (V_t) for coarse particle slurries was used to choose the data where only kinematic friction is important (i.e. negligible contact load friction). According to Wilson, V_t is the velocity at which the kinematic friction component of the slurry flow starts to dominate. When the operating velocity (V) is less than V_t, all particles travel as a sliding bed. At velocities greater than V_t, a progressively greater concentration particles is suspended. Wilson suggested when V>5V_t, a

complete turbulent suspension can be expected and only kinematic friction exists. The expression for V_t is:

$$V_t = 0.6 v_\infty \sqrt{\frac{8}{f_f}} e^{\frac{45 d_{50c}}{D}}$$

(5.1)

where v_∞ is the terminal settling velocity of a single particle, f_f is the Darcy friction factor for the carrier fluid, d_{50c} is average coarse particle diameter and D is the pipe diameter.

For the calculation of V_t for pet coke-water slurries at 70^0C, v_∞ was determined using **Haider and Levenspiel's (1989)** equation. They proposed a correlation to predict terminal settling velocity for spherical particles. The usage of this correlation is justified here because pet coke particles are not angular, as seen in the photograph of pet coke in **Gillies (2012)** and from its C_{max} value. The Darcy friction factor for the carrier fluid, f_f, was assumed to be the average of the friction factors in the velocity range over which hot water tests were conducted. The average coarse particle diameter for the pet coke was taken as its d_{85}. The threshold turbulent velocity (V_t) for the pet coke-water slurries tested at 70^0C was found to be 0.43 m/s or $5V_t$ to be 2.17 m/s. The experimental operating velocity range for hot water-pet coke tests was just above this velocity, ensuring that all the data points could be used for the f_s analysis.

2. The experimental water data at 70^0C were used to obtain a best polynomial fit for shear stress vs. velocity. From the fitted equation, baseline water friction (τ_f) at test velocities (velocities tested in the slurry runs) was determined.

3. Using the baseline water friction, the fluid friction factor was determined and used to calculate d^+ (Equation 2.20) at each velocity.

4. In Equation 2.14b, at high velocities, Coulombic friction (F_2) is negligible and $\tau_{1k}=\tau_{2k}=\tau_k$. Hence, experimental pressure gradients measured for the slurry runs were used to determine the slurry kinematic friction, τ_k. From Equation 2.17, it can be seen that subtracting the water friction, τ_f, from corresponding τ_k, the "solids related" friction τ_s was obtained. From the solids friction, the solids friction factor, f_s, was calculated. For the sake of comparison with the f_s correlation from the model, the experimental friction factors were made independent of solids concentration by dividing them by $\lambda^{1.25}$, where λ was calculated from Equation 2.19, using the coarse solids concentration from the Coriolis flow meter and the C_{max} value for pet coke.

It is worth noting here that model correlation for f_s had been developed for $0<d^+<80$ from previous tests with sand-water, alumina-water and pet coke-water with various solids concentrations and particle sizes (**Gillies, 2012**). Figure 5.13 shows the comparison of solid friction factors calculated using the data for pet coke-water slurries at 70^0C with the correlation for f_s used in the model.
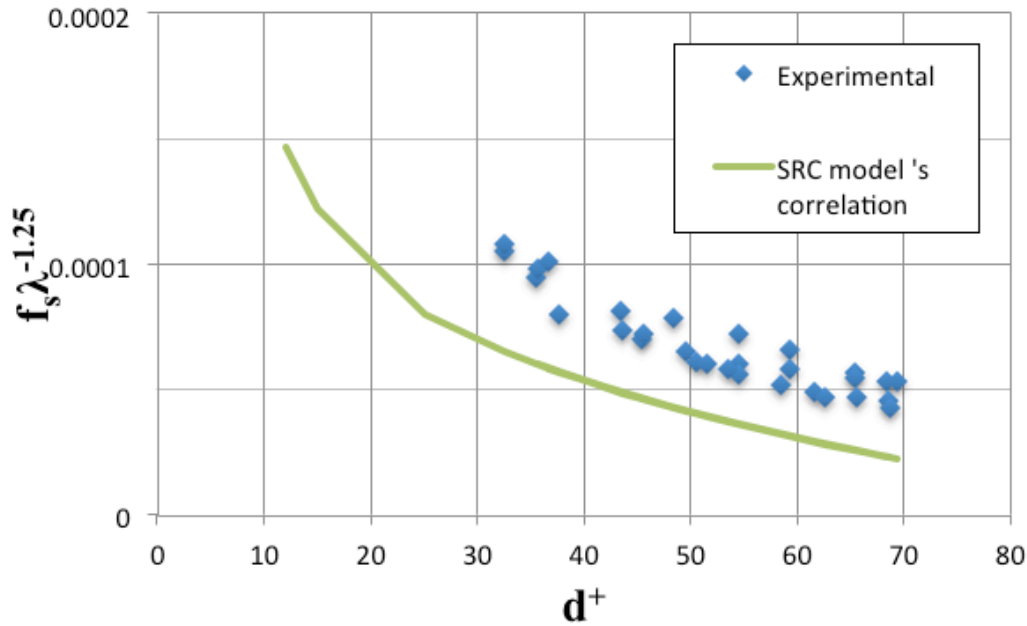
Figure 5.13 Comparison of experimental solid friction factors with the predicted solid friction factors for pet coke-water slurry: D=50mm; d_{50c}=131μm; T=70^{0}C

There was a consistent under-prediction from the SRC model's correlation with regards to the experimental solid friction factors for the entire test range of d^+. The under-prediction at higher velocities ($d^+>50$) is not understood at this time, as there seems to be no experimental clues suggesting why this occured. However, at lower velocities ($30<d^+<40$), it might be possible that some non-negligible Coulombic friction still exist due to the presence of some coarser particles in the slurry, thereby increasing the overall slurry friction (or causing the overestimation of f_s). This can be understood from Figure 5.14, where contact load fractions of 131μm and 300μm pet coke-hot water slurries at C_{vd}=0.25, as predicted from the SRC model, are shown over the velocity range of hot water slurry tests. It can be seen that the contact load fraction increases rapidly at lower velocities for coarser particles. Assuming that under-prediction from the SRC model's correlation with

regards to the experimental solid friction factors is real even for low velocities (no interference of Coulombic friction), then, the implication of this observed under-prediction on the SEC analysis for slurries with low carrier fluid viscosities needs to be determined. This implication is presented in the subsequent discussion.
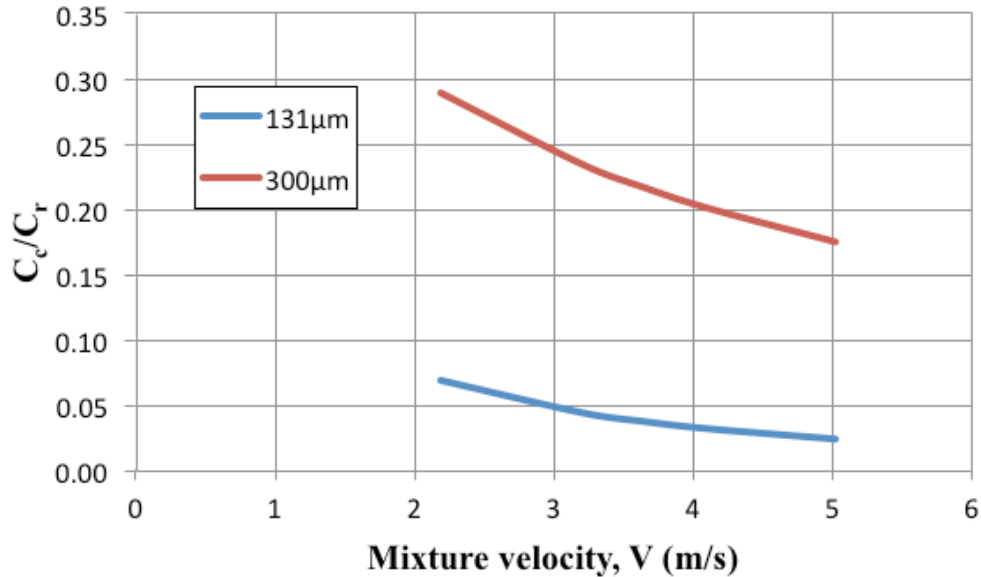
Figure 5.14 Comparison of predicted contact load fractions for two pet coke-water slurries: D=50mm; C_{vd}=0.25;T=70^{0}C

In Chapter 3, SEC analysis done for pet coke-liquid CO_2 in the 200mm pipeline was based on the hydraulic gradient predictions from the SRC model. These predictions are primarily dependent on the accuracy of the f_s correlation in the model for these slurries. To analyze the effect of the observed under-prediction of the f_s correlation (as seen from Figure 5.13) on the SEC analysis for slurries with low carrier fluid viscosities, Figure 5.15 is plotted. In Figure 5.15, SEC values calculated for pet coke-water slurries at 70^{0}C from the experimental data at a

given reference velocity (2.5m/s) are compared with the SEC predictions obtained using the SRC model.
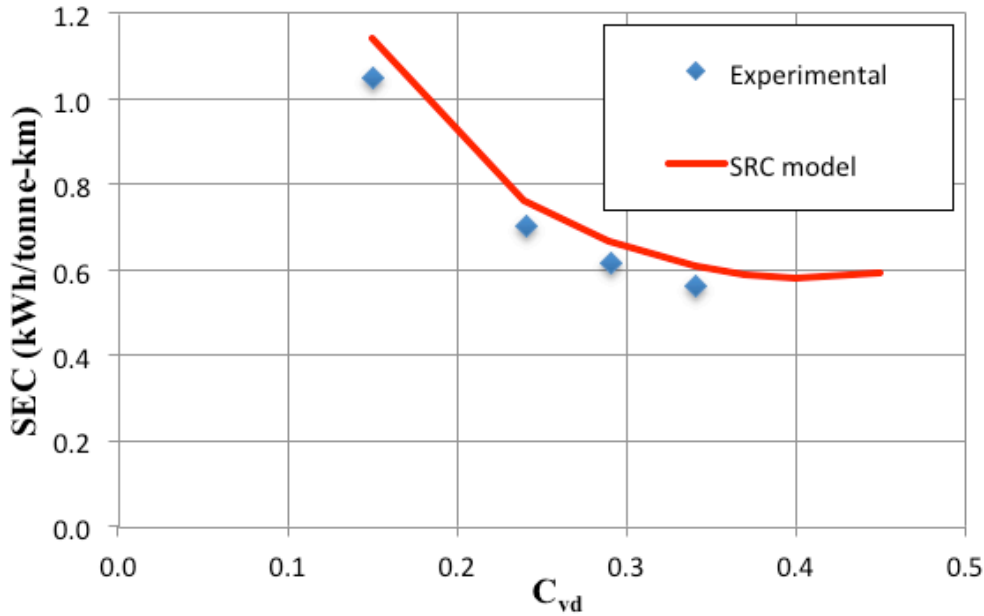
Figure 5.15 Comparison of SEC obtained from experimental data with predicted SEC for pet coke-water slurry: D=50mm; d_{50c}=131µm;V=2.5m/s; T=70^{0}C

It can be seen from Figure 5.15 that the model based SEC curve predicts optimum solids concentration (SEC minimum) to be around 40%. The trend of the experimental data also points towards this result. In Figure 5.15, the margin of error between the SEC predictions obtained from the model is, on average, 7.5% compared with the experimental data obtained in the present study. A similar margin of error was also found for other velocities. As the f_s correlation in the model is independent of pipe diameter, a similar margin of error can be expected in the SEC analysis done for pet coke-liquid CO_2 slurries (see Chapter 3).

5.5 Measuring technique for coefficient of friction

For slurries with coarser particles, the Coulombic friction component becomes important, which is evident from Figure 5.14. Therefore, in addition to kinematic friction, accurate Coulombic friction estimation is equally crucial to the reliability of the model predictions for a wide range of particle sizes. As seen in Equation 2.15, the coefficient of friction (η_s) is used in determining the Coulombic friction component of settling slurries in the SRC two-layer model. It is primarily dependent on the solid particle-pipe material interaction and it is one of the important characterization parameters required for prediction of friction losses for coarse-particle slurries. Currently, in the model, η_s is determined as follows (**Gillies et al., 2004**):

$$\eta_s = \eta_{s0} \left[2 \left(1 - \frac{\delta}{d} \right) \right] \tag{5.2}$$

where η_{s0} =0.5 is the default value used for sand slurries in steel pipes and δ is the viscous sublayer thickness. The basis for expressing η_s as a function of δ/d is that Coulombic friction has been seen to increase when particles are large in comparison with the viscous sublayer thickness. A constraint is placed on the ratio of δ/d in Equation 5.2, which is: $0.1 \leq [2(1- \delta/d)] \leq 1$.

To make the model more rigorous, it will be useful to develop a database of η_{s0} values for various solid particle-pipe material combinations. A user of the model could then choose the value of η_{s0} appropriate for their slurry pipe flow application, allowing them to obtain more accurate slurry friction loss predictions. Here the design of an apparatus that can be used to measure η_{s0} for various solid

particle-pipe material combinations is proposed. **Gratton and Defrancesco (2006)** used a simple setup to measure the coefficient of sliding friction between two materials. In their setup, as illustrated schematically in Figure 5.16, a solid rectangular body was made to slide on a given test surface by pulling the string connected to the body. The other end of the string was attached to a force sensor placed on a movable truck. The sensor and truck were connected, through another string, to an electric motor turning at a constant speed. The force sensor was connected through an interface to a computer, which logged the sliding friction force data versus time. The coefficient of sliding friction was then calculated from the ratio of the measured friction force to the normal force (weight of the body).
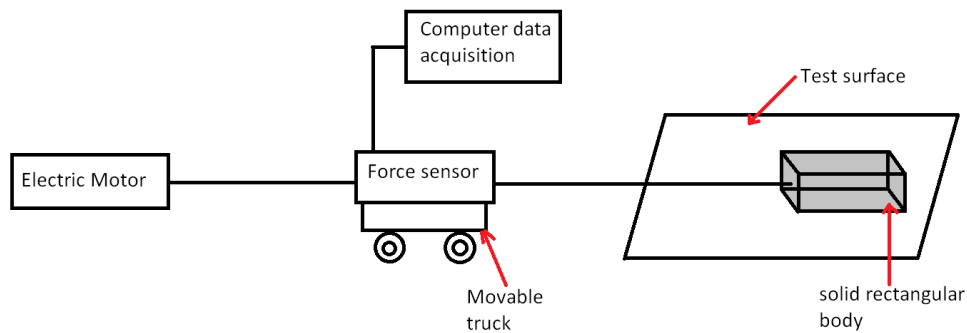
Figure 5.16 Schematic of the setup used to measure sliding coefficient of friction between two solid surfaces by Gratton and Defrancesco (2006)

In order to measure the coefficient of sliding friction for a sliding mass of solid particles on a given surface, the following modification is proposed. During the fabrication stage of the rectangular body, its base will be removed to obtain a

rectangular test cell, inside which solid particles of a given size can be placed, as illustrated in Figure 5.17.

Rectangular Test Cell with baseplate

Rectangular Test Cell without baseplate
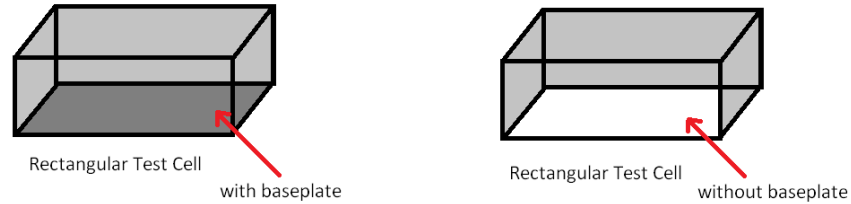
Figure 5.17 Illustration of base plate removal from the rectangular body for sliding coefficient of friction measurement of solids

The test cell will be then dragged at a constant speed by the turning motor. In this process, the solid particles inside the cell will come into sliding contact with the test surface and the sliding coefficient of friction can be measured from the following equation:

$$\eta_{s0} = \frac{F_s - F_0}{W} \tag{5.3}$$

where, F_s is the measured sliding friction force for the test cell filled with solid particles, F_0 is the measured sliding friction for test cell alone and W is the weight of the particles inside the test cell. The main design consideration during the fabrication of the cell will be to ensure that the material used for the test cell is heavier (or much higher density) than the sample of solid particles inside it. This will prevent possible spillage of the particles from the cell during the sliding process. Also, the edges of the cell will need to be coated with Teflon so that

$F_0 \ll F_s$. It needs to be seen whether variation in sliding velocity has an effect on the coefficient of friction.

Overall, the proposed apparatus offers the following advantages:

1. It is very inexpensive to fabricate;

2. Measurements can be done in a very short period of time;

3. The setup offers flexibility to test multiple solid particle-combinations by simply changing the test surface and adding the desired type of solids into the rectangular test cell.

6 Conclusions and Recommendations

6.1 Novel contributions of the present study

A detailed SEC analysis has been performed in this study to evaluate the optimum operating conditions, especially particle size and solids concentration, for pet coke-liquid CO_2 slurries and sulfur-liquid CO_2 slurries in a hypothetical 200mm (diameter) pipeline. These operating conditions would ensure the solids are transported at optimal energy consumption conditions. This study could be used directly as part of an engineering feasibility study for a pilot or industrial scale CO_2 slurry pipeline. The ability of the most current SRC two-layer model (PipeFlow 10) to predict friction losses for settling slurries with low carrier fluid viscosities was evaluated. Specifically, the performance of the kinematic friction correlation in the model was evaluated with the experimental friction loss data from pet coke slurry tests conducted at 70^0C in the 50mm loop. A novel technique to measure coefficient of friction for any combination of particles and pipe material was proposed. This will be valuable for any settling slurry applications where Coulombic friction is important.

6.2 Conclusions

Based on the anticipated available volume of liquid CO_2 for transport, optimum particle size and the predicted deposition velocities of these particles, an optimum pipe diameter (or near-optimum) of 200mm was proposed. The SEC analysis conducted for liquid CO_2 slurries of pet coke or sulfur in this pipe size suggested that the minimum SEC (and therefore optimum slurry pipeline operating

conditions) occur at a particle size of 100-150μm, a solids concentration of approximately 30% by volume and at a flow velocity of V=1.1V$_c$. While transport of smaller particles would actually reduce the SEC, particles smaller than 100-150μm become very difficult and inefficient to separate, thus risking commodity losses and contamination of CO_2 at the separation point.

It was determined that Coulombic friction is negligible and kinematic friction is dominant at higher operating velocities for liquid CO_2 slurries with particle sizes in the range of 100-150μm. However, if the particle size was increased even slightly, the Coulombic friction mechanism becomes important. Based on the experiments conducted with pet coke slurries in hot (70^{0}C) water, it was found that the existing kinematic friction correlation in the SRC model may slightly under-predict friction losses. Additional pipe-flow data sets on slurries with low carrier fluid viscosities are required before one can confirm the observed under-prediction. Based on the experiments conducted with pet coke slurries in hot (70^{0}C) water, it appears that actual values of the minimum SEC may be around 10% lower than the predicted values. However, the actual trends of SEC with particle size and solids concentration remain essentially unchanged. It needs to be noted that SEC values derived for liquid CO_2 slurries in this study cannot be directly used for other slurry systems. However the approach of obtaining SEC values from the SRC model and minimizing them with respect to a given operating condition (keeping other operating conditions constant) is still valid for other slurry systems.

6.3 Recommendations for future work

For future study, slurries prepared with low-viscosity carrier fluids such as hotter water (water at 80^0C) and triethylamine can be tested in the 50mm loop. This will expand the experimental database of settling slurries with low carrier fluid viscosities. The existing loop can be lengthened so that there is no flow disturbance from the elbow for Test Section 2. As a result, both test sections can be used for accurate friction loss measurements and measurement from either section can be used for the purpose of verification.

Bench-scale tests can be conducted to investigate the corrosion of stainless steel by sulfur-hot water mixtures. If the corrosion seen is less, then 100-150μm sulfur-hot water slurries can be tested in the 50mm loop over a wide range of concentrations. It would be then interesting to evaluate the performance of the f_s correlation in the model for sulfur-hot water slurries and subsequently analyze the error in the model's SEC prediction for those slurries.

It would be worth looking for methods to augment the viscosity of liquid CO_2. If any method is found, deposition velocity of solids in liquid CO_2 will be greatly reduced, which would reduce the minimum operating velocity for any liquid CO_2 slurry for a given pipe size, particle size and solids concentration. This would reduce SEC further for liquid CO_2 slurries.

7   References

"Accelerating Carbon Capture and Storage Implementation in Alberta", Report from Alberta Carbon Capture and Storage Development Council, March 2009.

"Appendix K Quantifying the GHG Reduction Benefits from the Quest CCS Project", Report from Shell Canada Limited, November 2010.

"CCS-Reducing the oil sands' carbon footprint", Report from ICO_2N, November 2011.

"Canada's Emission Trends", Report from Environment Canada, August 2012.

"ST98-2012: Alberta's Energy Reserves 2011 and Supply/Demand Outlook 2012– 2021", Report from Energy Resources Conservation Board, June 2012.

Barrie, J., K. Brown, P.R. Hatcher and H.U. Schellhase, "Carbon dioxide pipelines: A preliminary review of design and risks", Proceedings of the 7th International Conference on Greenhouse Gas Control Technologies, Vancouver, Canada (2004).

Bremer, J, "Pipeline flow of settling slurries", Presentation to Institution of Engineers Australia, 23 April (2008).

Churchill, S.W., "Friction factor equation spans all fluid regimes," Chem. Eng. 84(24), 91-92 (1977).

Colwell, J.M. and C.A. Shook, "The entry length for slurries in horizontal pipeline flow", Can. J. Chem. Eng. 66, 714-720 (1988).

Darby, R., R. Mun, and D.V. Boger. "Predict friction loss in slurry pipes", Chem. Eng. 99(9), 116-119 (1992).

Davies, J. T. "Calculation of critical velocities to maintain solids in suspension in horizontal pipes", Chem. Eng. Sci. 42, no. 7, 1667-1670 (1987).

Duschek, W., R. Kleinrahm, and W. Wagner. "Measurement and correlation of the (pressure, density, temperature) relation of carbon dioxide I. The homogeneous gas and liquid regions in the temperature range from 217 K to 340 K at pressures up to 9 MPa", The Journal of Chemical Thermodynamics 22, no. 9, 827-840 (1990)

Fang, H., D.Young and S Nešić, "Corrosion of mild steel in the presence of elemental sulfur", NACE Corrosion Conference and Expo, Paper No 08637 (2008).

Fenghour, A., W.A. Wakeham, and V. Vesovic. "The viscosity of carbon dioxide", Journal of Physical and Chemical Reference Data 27, no. 1, 31-44, (1998).

Gillies, D.P., Particle Contributions to Kinematic Friction in Slurry Pipeline Flow, *University of Alberta: M.Sc. Thesis, Dept. of Chemical Engineering* (2012).

Gillies, R.G., Pipeline Flow of Coarse Particle Slurries, *University of Saskatchewan: Ph.D. Thesis, Department of Chemical Engineering* (1993).

Gillies, R.G., *Pipeline Flow of Settling Slurries: A Summary of Recent Innovations*. SRC Publication No. 11606-1E03, (2003).

Gillies, R.G., C.A. Shook and J. Xu, "Modelling heterogeneous slurry flows at high velocities", Can. J. Chem. Eng. 82, 1060-1065 (2004).

Gillies, R.G. and C.A. Shook, "Modelling high concentration settling slurry flows", Can. J. Chem. Eng. 78, 709–716 (2000).

Gillies, R.G., C.A. Shook and K.C. Wilson, "An improved two-layer model for horizontal slurry pipeline flow", Can. J**.** Chem. Eng. 69, 173-178 (1991).

Gratton, L.M. and S. Defrancesco, "A simple measurement of the sliding friction coefficient", Physics Education, 41, 232-235 (2006).

Haider, A. and O. Levenspiel, "Drag coefficient and terminal velocity of spherical and nonspherical particles", Powder Technology, 58, 63–70 (1989).

Hashemi, S.A., R.S. Sanders and K.C. Wilson, "Specific energy consumption and desirable operating conditions for fine-particle slurries", 18th International Conference on Hydrotransport, Rio de Janeiro, Brazil, 22 – 24 September, pp. 5-15 (2010).

Kadry S, "Corrosion analysis of stainless steel", European Journal of Scientific Research, Vol 22, No 4, 508-516 (2008).

Li, H, "Thermodynamic Properties of CO_2 Mixtures and Their Applications in Advanced Power Cycles with CO_2 Capture Processes", *KTH, Royal Institute of Technology, Ph.D. Thesis, Department of Chemical Engineering and Technology* (2008)

Luhning, R.,"CO_2 slurry pipeline to transport solid marketable products to improve CCS economics", World Energy Congress, Montreal (2010).

Luhning, R., "CO$_2$ transportation options", Presentation to Petroleum Technology Alliance of Canada, Calgary, Alberta, October 15 (2012).

McCoy, S.T. and E.S. Rubin, "An engineering-economic model of pipeline transport of CO$_2$ with application to carbon capture and storage", International Journal of Greenhouse Gas Control 2, no. 2, 219-229 (2008).

Ng, S.H. and S.N. Bhattacharya, "The transport of brown coal-liquid carbon dioxide slurries in small pipes", Chemeca 88: Australia's Bicentennial International Conference for the Process Industries (1988).

Park, Sang Huck. Separation of polymer particles using a hydrocyclone, *Lehigh University: MSc thesis, Department of Polymer Science and Engineering* (2003).

Pullum, L. and D.J.M. McCarthy, "Ultra high concentration and hybrid hydraulic transport systems", Freight Pipelines. In: Round, G.F. (Eds.), pp. 127–139 (1993).

Santhanam, C.J., "Coal/liquid CO$_2$ slurry technology status", The 8th International Conference on Slurry Transportation, San Francisco, California, March 15-28 (1983).

Santhanam, C.J., S.E. Dale, J.F. Peirson and W.J Burke, "Development of low rank-coal/liquid CO_2 slurries: A status report", Proc. EPRI Contractor's Conference on Coal Gasification, Palo Alto, California (1984).

Schaan, J.J., Pipeline Flow of Newtonian Fine Particle Slurries. *University of Saskatchewan: M.Sc. Thesis, Dept. of Chemical Engineering* (2001).

Schaan, J., R.J. Sumner, R.G. Gillies, and C.A. Shook, "The effect of particle shape on pipeline friction for Newtonian slurries of fine particles", Can J. Chem. Eng. 78, 717-725 (2000).

Shook, C.A., R.G. Gillies, and R.S. Sanders, *Pipeline Hydrotransport with Applications in the Oil Sand Industry,* Saskatchewan Research Council, Saskatoon, Canada, SRC Publication 11508-1E02 (2002).

Shook, C.A. and M.C. Roco, *Slurry Flow Principles and Practice*, Butterworth-Heinemann (1991).

Singh, S.N., V. Seshadri, R. Mishra, and C. Fabien, "Settled bed characteristics in a multisized particulate solid-liquid suspension", Powder Handling & Processing 13, 191-196 (2001).

Spelay, R., S.A. Hashemi, D.P. Gillies, R. Hegde, R.G. Gillies and R.S. Sanders, "Governing friction loss mechanisms and the importance of off-line characterization tests in the pipeline transport of dense coarse-particle slurries", Proceedings of the ASME 2013 Fluids Engineering Summer Meeting, July 7-11, Incline Village, Nevada, USA (2013).

Thomas, D.G., "Transport characteristics of suspensions: VII. A note on the viscosity of Newtonian suspensions of uniform spherical particles", J. Colloid Sci. 20, 267-277 (1965).

Wasp, E.J., Aude, T.C., Kenny, J.P. and P.B Williams, "Deposition velocities, transition velocities and spatial distribution of solids in slurry pipelines", Proc. Hydrotransport 1, BHRA Fluid Engineering, Cranfield U.K., Paper H4, 53-76 (1970).

Wilson, K.C., Addie, G.R., Sellgren, A. and R. Clift, *Slurry Transport Using Centrifugal Pumps*, 3rd Ed. Elsevier Applied Science, (2006).

Wilson, K.C., "A unified physically based analysis of solid-liquid pipeline flow", in Proc. 4th Int. Conf. on Hydraulic Transport of Solids, H.S. Stephans, Ed., Banff, May 18-21, BHRA Fluid Engineering, Cranfield, UK, Paper Al, pp. 1-16 (1976).

Wilson, K.C., "Deposition-limit Nomograms for particles of various densities in pipeline flow", In Proc. Hydrotransport 6, BHRA Fluid Engineering, Cranfield, U.K., pp. 1-12 (1979).

Wilson, M. and M. Monea, "IEA GHG Weyburn CO_2 monitoring and storage project summary report 2000-2004", Proceedings of the 7th International Conference on greenhouse gas control technologies, 5-9 September, Vancouver, Canada (2004).

Wu. J, L. Graham, S. Wang and R. Parthasarathy, "Energy efficient slurry holding and transport", Minerals Engineering, 23, 705–712(2010).

Yuchi, W, B. Li., W. Li and H. Chen, "Effects of coal characteristics on the properties of coal water slurry", Coal Preparation, 25:4, 239-249 (2005).

Zhang, Z.X., G.X. Wang, P. Massarotto and V. Rudolph. "Optimization of pipeline transport for CO_2 sequestration", Energy Conversion and Management 47, no. 6, 702-715 (2006).

APPENDICES

Appendix A: Particle size distributions and settled bed concentrations

LM 125 sand	
Particle Diameter (µm)	Volume % below
1000	100
425	98.04
300	96.9
212	94.8
150	84.95
125	73.02
106	58.83
90	43.99
75	29.31
63	18.64
53	11.48
45	7.24
38	4.56

Petroleum coke	
Particle Diameter (μm)	Volume % below
1000	100
425	96.95
212	86.95
150	63.89
125	48.04
106	34.76
90	24.2
75	15.74
63	10.22
53	6.51
45	4.16
38	2.56

LM 70 sand	
Particle Diameter (μm)	Volume % below
1000	100
425	95.55
300	87.11
212	65.45
150	38.11
125	25.1
106	15.67
90	9.06
75	4.62
63	2.37
53	1.23
45	0.68
38	0.37

Raw data for settled bed concentration for LM 125 sand:

For 30% by volume sample, 170.357g of sand mixed with 150ml of water.

Measured settled bed volume= 128 ml.

Volume of the particles= 64.15ml

$$C_{max} = \frac{64.15}{128} = 0.50$$

Raw data for settled bed concentration for LM 70 sand:

For 30% by volume sample, 227.14g of sand mixed with 200ml of water.

Measured settled bed volume= 166 ml.

Volume of the particles= 85.66ml

$$C_{max} = \frac{85.66}{166} = 0.516$$

Raw data for settled bed concentration for Petroleum coke:

For 30% by volume sample, 137.14 g of sand mixed with 220ml of water.

Measured settled bed volume = 144 ml.

Volume of the particles= 85.71ml

$$C_{max} = \frac{85.71}{144} = 0.60$$

Appendix B: Experimental Pipeline pressure Gradients

Pipeline flow data for water from Test Section 1 and Test Section 2 in 53mm diameter pipeline

Data collector: Rajesh Hegde
Temperature: 25°C
Pipe Diameter: 0.0528 m

Test section 1			Test Section 2 (0.48m from elbow)			Test Section 2 (0.32m from elbow)		
Velocity (m/s)	-dP/dz (Pa/m)	Density (kg/m^3)	Velocity (m/s)	-dP/dz (Pa/m)	Density (kg/m^3)	Velocity (m/s)	-dP/dz (Pa/m)	Density (kg/m^3)
0.69	104.07	997.5	0.64	104.59	997.5	0.69	144.68	997.5
1.01	203.43	997.5	0.85	173.99	997.5	1.01	290.23	997.5
1.32	328.76	997.5	1.05	260.48	997.5	1.32	478.60	997.5
			1.30	382.29	997.5			
1.58	458.16	997.5	1.54	526.51	997.5	1.58	675.27	997.5
1.99	696.39	997.5	1.79	698.90	997.5	1.99	1045.94	997.5
			2.04	890.15	997.5			
2.25	875.45	997.5	2.24	1054.80	997.5	2.25	1330.39	997.5
2.56	1117.29	997.5	2.47	1275.72	997.5	2.56	1713.39	997.5
2.86	1374.36	997.5	2.68	1487.80	997.5	2.86	2135.63	997.5
3.17	1653.18	997.5	2.81	1624.53	997.5	3.17	2601.00	997.5
			2.98	1814.63	997.5			
3.45	1925.86	997.5	3.21	2087.94	997.5	3.45	3076.36	997.5

Pipeline flow data for 96μm (LM 125) in 53mm diameter pipeline

Data collector: Rajesh Hegde
Temperature: 21°C
Pipe Diameter: 0.0528 m

Solids concentration (v/v %)								
5%			10%			15%		
Velocity	-dP/dz	Density	Velocity	-dP/dz	Density	Velocity	-dP/dz	Density
(m/s)	(Pa/m)	(kg/m^3)	(m/s)	(Pa/m)	(kg/m^3)	(m/s)	(Pa/m)	(kg/m^3)
1.41	460.98	1083	1.45	541.80	1165	1.50	651.01	1249
1.64	586.54	1083	1.62	651.10	1170	1.64	738.90	1249
1.91	758.18	1083	1.89	830.39	1173	1.91	929.84	1252
2.14	920.61	1083	2.11	1000.53	1176	2.13	1111.42	1256
2.37	1101.15	1083	2.34	1185.40	1177	2.36	1308.74	1260
2.59	1286.56	1083	2.57	1391.69	1179	2.60	1531.19	1261
2.77	1447.28	1083	2.75	1563.77	1183	2.79	1712.19	1262
2.96	1619.23	1083	2.94	1744.78	1183	2.97	1893.94	1263

Pipeline flow data for 174µm sand (LM 70) in 53mm diameter pipeline

Data collector: Rajesh Hegde
Temperature: 21°C
Pipe Diameter: 0.0528 m

Solids concentration (v/v %)								
15%			25%			30%		
Velocity	-dP/dz	Density	Velocity	-dP/dz	Density	Velocity	-dP/dz	Density
(m/s)	(Pa/m)	(kg/m^3)	(m/s)	(Pa/m)	(kg/m^3)	(m/s)	(Pa/m)	(kg/m^3)
1.52	942.00	1420	1.52	942.00	1420	1.51	1224.80	1520
1.62	1008.64	1420	1.62	1008.64	1420	1.59	1261.15	1520
1.84	1186.68	1422	1.84	1186.68	1422	1.78	1431.10	1520
2.06	1388.87	1426	2.06	1388.87	1426	2.00	1634.99	1521
2.19	1517.88	1429	2.19	1517.88	1429	2.18	1819.50	1523
2.37	1693.75	1432	2.37	1693.75	1432	2.36	2011.02	1523
2.56	1890.32	1432	2.56	1890.32	1432	2.54	2221.77	1526
2.73	2083.34	1435	2.73	2083.33	1435	2.68	2375.57	1526
			2.78	2132.51	1435	2.90	2645.82	1527

Pipeline flow data for 128μm petroleum coke in 53mm diameter pipeline

Data collector: Rajesh Hegde
Temperature: 21°C
Pipe Diameter: 0.0528 m

Solids concentration (v/v %)								
16%			32%			37%		
Velocity	-dP/dz	Density	Velocity	-dP/dz	Density	Velocity	-dP/dz	Density
(m/s)	(Pa/m)	(kg/m^3)	(m/s)	(Pa/m)	(kg/m^3)	(m/s)	(Pa/m)	(kg/m^3)
			1.04	489.10	1192			
0.91	319.42	1096				1.42	1027.25	1223
			1.22	583.75	1192			
1.08	358.91	1097				1.60	1133.10	1220
			1.44	717.05	1194			
1.21	457.69	1097				1.83	1302.91	1226
			1.72	901.86	1194			
1.69	638.29	1100				2.15	1558.09	1230
			2.00	1145.12	1198			
1.92	791.56	1100				2.38	1758.80	1231
			2.28	1350.08	1200			
2.19	1008.80	1104				2.66	2020.00	1232
			2.39	1513.60	1200			
2.51	1285.17	1107				2.90	2259.64	1233
			2.67	1762.29	1202			
2.77	1522.75	1108				3.27	2643.45	1234
			2.89	1944.20	1203			
3.04	1804.53	1108						
			3.08	2146.47	1204			

Pipeline flow data for 128μm petroleum coke in 53mm diameter pipeline

Data collector: Rajesh Hegde
Temperature: 70°C
Pipe Diameter: 0.0528 m

Solids concentration (v/v %)					
15%			25%		
Velocity	dP/dz	Density	Velocity	-dP/dz	Density
(m/s)	(Pa/m)	(kg/m^3)	(m/s)	(Pa/m)	(kg/m^3)
2.18	707.28	1073	2.17	761.09	1134
2.56	930.50	1070	2.40	892.83	1133
2.99	1248.01	1075	3.14	1423.26	1136
3.36	1546.29	1075	3.44	1674.04	1136
3.81	1942.25	1075	3.81	2014.98	1135
4.18	2298.28	1075	4.17	2386.00	1136
4.63	2774.98	1075	4.63	2893.54	1136
4.85	3022.50	1075	4.93	3250.21	1136

Pipeline flow data for 128 micron petroleum coke in 53mm diameter pipeline

Data collector: Rajesh Hegde
Temperature: 70°C
Pipe Diameter: 0.0528 m

Solids concentration (v/v %)					
30%			35%		
Velocity (m/s)	dP/dz (Pa/m)	Density (kg/m^3)	Velocity (m/s)	-dP/dz (Pa/m)	Density (kg/m^3)
2.41	953.92	1168	2.48	1077.45	1196
3.00	1369.81	1168	3.15	1571.74	1196
3.51	1806.58	1173	3.59	1948.92	1195
3.81	2086.20	1173	3.74	2112.34	1201
4.34	2630.09	1174	4.11	2482.61	1201
4.64	2973.61	1175	4.42	2810.53	1201
4.87	3246.80	1175	4.87	3336.75	1201

Appendix C: Input parameters and their values to obtain SRC two-layer model predictions for SEC calculations

Input parameters and values to obtain SRC model predictions for 174μm sand-water at 19^{0}C

Input parameters	Values
Pipe internal diameters (m)	0.05-0.5
Pipe wall roughness (mm)	0.01
Pipeline Slope (degrees)	0
Coarse solids particle size (mm)	0.174
Coarse solids density (kg/m^3)	2650
Solids concentration specified	Delivered
Solids settled bed concentration	0.505
Carrier fluid density (kg/m^3)	998
Carrier fluid viscosity (mPa.s)	1.00

Input parameters and values to obtain SRC model predictions for pet coke-liquid CO_2

Input parameters	Values
Pipe internal diameters (m)	0.05-0.5
Pipe wall roughness (mm)	0.01
Pipeline Slope (degrees)	0
Coarse solids particle size (mm)	0.075-1
Coarse solids density (kg/m^3)	1600
Solids concentration specified	Delivered
Solids settled bed concentration	0.61
Carrier fluid density (kg/m^3)	867
Carrier fluid viscosity (mPa.s)	0.1

Input parameters and values to obtain SRC model predictions for 128μm pet coke-water at 70^{0}C

Input parameters	Values
Pipe internal diameters (m)	0.0528
Pipe wall roughness (mm)	0.01
Pipeline Slope (degrees)	0
Coarse solids particle size (mm)	0.131
Coarse solids density (kg/m^3)	1600
Solids concentration specified	Delivered
Solids settled bed concentration	0.61
Carrier fluid density (kg/m^3)	977
Carrier fluid viscosity (mPa.s)	0.39

Sample Screen shot of Inputs and Outputs of the SRC two-layer model (Pipe Flow 10)

PipeFlow 10

smart science solutions

This model applies to the turbulent flow of settling slurries.

Run PipeFlow Model

Inputs

Mixture Volumetric Flowrate (m³/s)	Pipe Internal Diameter (m)	Pipe Wall Roughness (mm)	Pipeline Slope (degrees)	Coarse Solids Volume Fraction in:		In-situ or Delivered ?	Coarse Particle Properties:		Carrier Properties:		Pipeline Velocity (m/s)
				Settled Bed	Mixture		Density (kg/m³)	d_{50} (mm)	Density (kg/m³)	Viscosity (mPa·s)	
0.065	0.2	0.01	0.00	0.61	0.300	d	1600	0.075	867	0.10	2.07
0.068	0.2	0.01	0.00	0.61	0.300	d	1600	0.075	867	0.10	2.16
0.079	0.2	0.01	0.00	0.61	0.300	d	1600	0.075	867	0.10	2.51
0.09	0.2	0.01	0.00	0.61	0.300	d	1600	0.075	867	0.10	2.86
0.11	0.2	0.01	0.00	0.61	0.300	d	1600	0.075	867	0.10	3.50
0.15	0.2	0.01	0.00	0.61	0.300	d	1600	0.075	867	0.10	4.77

Model Predictions

Contact Load Fraction, Cc/Cr	Deposition Velocity (m/s)	Pipeline Pressure Gradient (Pa/m)	In Situ Mixture		Delivered Mixture		Parameters which are outside the range of the database:
			Density (kg/m³)	Coarse Solids Vol Fraction	Density (kg/m³)	Coarse Solids Vol Fraction	
0.041	2.00	147	1092	0.308	1087	0.300	Viscosity
0.038	2.00	154	1092	0.307	1087	0.300	Viscosity
0.031	2.00	185	1090	0.305	1087	0.300	Viscosity
0.026	2.00	223	1089	0.304	1087	0.300	Viscosity
0.019	2.00	308	1089	0.302	1087	0.300	Viscosity
0.011	2.00	547	1088	0.301	1087	0.300	Viscosity

Appendix D: Input parameters and their values to obtain SRC two-layer model predictions for slurry tests at room temperature
Input parameters and values to obtain SRC model predictions for 96µm sand-water at 21^{0}C

Input parameters	Values
Pipe internal diameter (m)	0.0528
Pipe wall roughness (mm)	0.01
Pipeline Slope (degrees)	0
Coarse solids particle size (mm)	0.100
Coarse solids density (kg/m^3)	2650
Solids concentration specified	Delivered
Solids settled bed concentration	0.50
Carrier fluid density (kg/m^3)	1019-1021
Carrier fluid viscosity (mPa.s)	1.23

Input parameters and values to obtain SRC model predictions for 174µm sand-water at 21^{0}C

Input parameters	Values
Pipe internal diameter (m)	0.0528
Pipe wall roughness (mm)	0.01
Pipeline Slope (degrees)	0
Coarse solids particle size (mm)	0.174
Coarse solids density (kg/m^3)	2650
Solids concentration specified	Delivered
Solids settled bed concentration	0.505
Carrier fluid density (kg/m^3)	1001-1003
Carrier fluid viscosity (mPa.s)	1.00

Input parameters and values to obtain SRC model predictions for 128μm pet coke-water at 21⁰C

Input parameters	Values
Pipe internal diameter (m)	0.0528
Pipe wall roughness (mm)	0.01
Pipeline Slope (degrees)	0
Coarse solids particle size (mm)	0.131
Coarse solids density (kg/m^3)	1600
Solids concentration specified	Delivered
Solids settled bed concentration	0.60
Carrier fluid density (kg/m^3)	1002
Carrier fluid viscosity (mPa.s)	1.23

Appendix E: Technical specifications and drawings of the equipments/ instruments in the 50 mm loop

Coriolis flow meter specifications (Spartan Controls Product Data sheet, PS-00603, Rev.M)

Sensor model #: F200S418C2BAEZZZZ (Micromotion F series model)

Transmitter model #: 2700R12BBAEZZZ

Calibration method: Flow meter calibrated with air and water at 22^0C

Flow meter accuracy: 0.2% of mass flow rate and ±2 kg/m^3 for density

Pressure and temperature ratings: 64 psig, maximum process temperature of 204^0C and maximum ambient temperature for core processor/transmitter is 60^0C

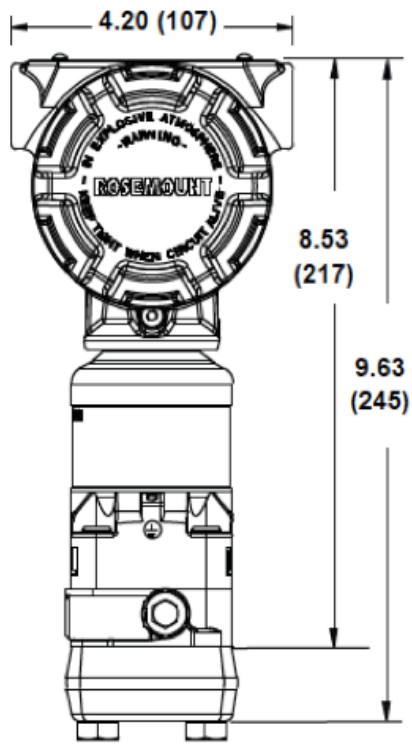Maximum permissible flow rate and density: 24.19 kg/s and 5000 kg/m^3

Transmitter output: One active 4-20mA output

Coriolis flow meter drawing (Spartan Controls Product Data sheet, PS-00603, Rev.M)
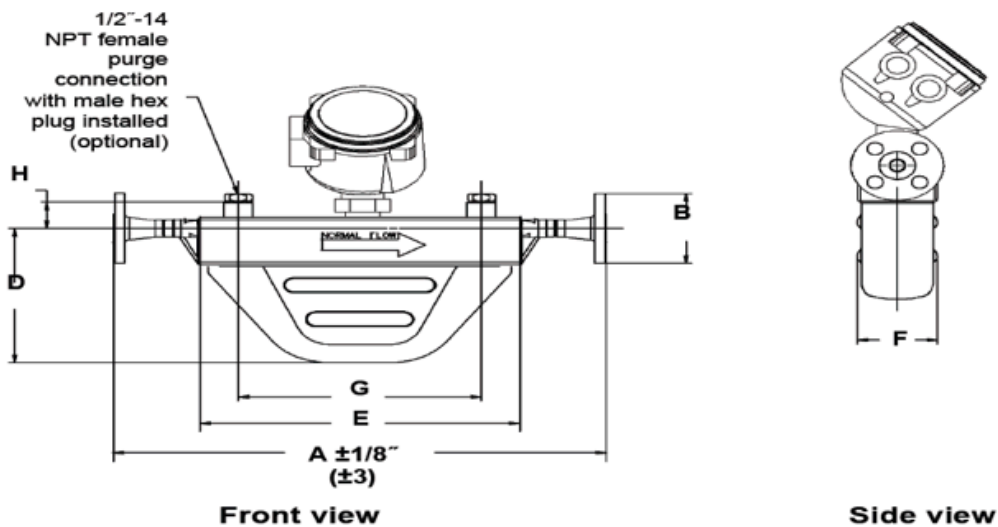
Model	No. of flow tubes	Units	Flow tube ID	Dimensions						
				A	B	D	E	F	G	H
F200	2	in	1.1	24.88	6	12.56	17.88	5.62	14	2.38
		mm	27	632	152	319	454	143	356	61

Differential pressure transducer drawing (Spartan Controls Product Data sheet, 00813-0100-4801, Rev PA)

4.20 (107)

8.53 (217)

9.63 (245)

Front view

Dimensions are in inches (millimeters)

4.55 (116)

FIELD
TERMINALS

6.44 (164)
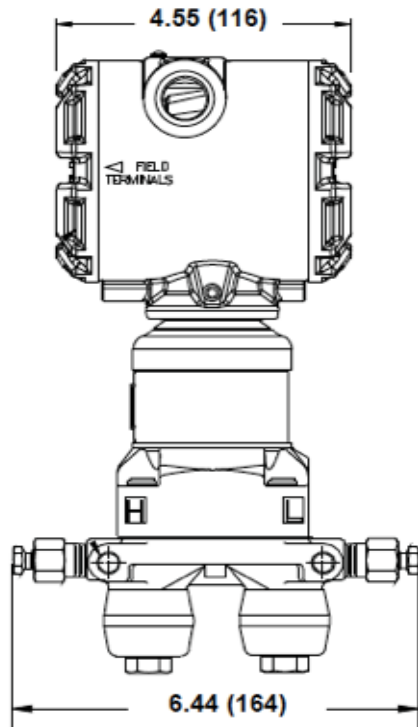
Side view

Dimensions are in inches (millimeters)

Differential pressure transducer specifications: (Spartan Controls Product

Data sheet, 00813-0100-4801, Rev PA)

Model #: 3051S1CD1A2E12A1AB4D1D2K6M5 (Rosemount Differential

Pressure Transmitter)

Measurement range: 0 to 25 inches of water

Accuracy: 0.09% of the full span range (i.e. 0.09% of 25 inches of water)

Transmitter output: 4-20 mA w/digital signal based on HART protocol

Immersion heater specifications: (CCI Thermal technologies Inc)

Model No: CXCT345P2

Heating capacity: 4.5 kW, Immersion length: 12".

Thermostat range: 10^0C to 120^0C

Temperature probe specifications: (Omega Canada)

1/16''ID and 12'' long K-type thermocouple probe made of SS 304.

Data acquisition specifications: (National Instruments)

Central data acquisition unit: NI cDAQ-9174, 4-Slot USB Chassis (only two slots used)

One slot for NI 9203, 8-Channel ±20 mA, 200 kS/s, 16-Bit Analog Current Input module (2 channels used for the two differential pressure transmitters and one channel used for the Coriolis flow meter transmitter)

One slot for NI 9211, 4-Channel, 14 S/s, 24-Bit, ±80 mV Thermocouple Input Module (One channel used for the thermocouple probe)

Moyno pump specifications, sizing calculations and pump curve:

Pump Model #: 2F090G1CDB3SAC (Progressing Cavity Pump 2000 Series)

Pump Description: 2 Stage pump, Castings-Iron, Rotor-Undersize chrome plated, Internals-Alloy, Stator-EPDM, Shaft Seal-Single Mechanical seal, Suction: 8'' 150LB ANSI Flat Faced Flange, Discharge: 8'' 150LB ANSI Flat Faced Flange

Motor (from Baldor): 10 HP motor, 1750RPM. Rated for 3phase, 60Hz, 208/230V supply. Motor is also explosion-proof rated and capable of continuous VFD duty. Gearbox ratio=10.4 (1750/168).

VFD (from Alberta Industrial Control and Drives): Model# VS1GV210-1B. Rated for 230/208V, 3phase supply on a 10HP motor with maximum continuous duty of 28A.

Pump sizing calculations:

For sizing and selection of the pump, maximum pressure head and flow rate were calculated and given to the vendor (Wajax Industrial Components). Based on the maximum head and flowrate, maximum pumping power was calculated for choosing the power capacity of the motor.

Maximum flow rate= 9.2 liters/s (linear velocity of 4.2m/s)

Maximum frictional pressure loss was based on frictional pressure gradient prediction from the SRC two layer model for 35% sand-water slurry (d_{50}=1mm) flowing in 2'' pipe at V=4.2m/s and T=19^{0}C. From the model prediction, frictional pressure gradient for sand-water slurry was 7738 Pa/m.

$$Max\ hydraulic\ gradient = \frac{7738}{9.8*998} = 0.791\frac{m\ water}{m\ pipe}$$

Taking total pipe loop length of 12m, total friction loss in the system was 9.5 meters of water (0.791*12). To account for uncertainties, a safety factor of 2 was multiplied with this value. Final value of maximum head was taken as 20m of water (196kPa). The pair of design flow rate (9.2 liters/s or 33.12 m^3/hr) and design head (20m of water or 28.42 psi) was given to the vendor.

For sizing the motor, required pumping power was calculated as follows using a conservative pump efficiency of 30%:

$$P = \frac{\Delta P * Q}{\eta} = \frac{196000 * 9.2 * 10^{-3}}{0.3} = 6.01 kW = 8.06 HP$$

Based on the above pumping power requirement, a 10HP motor was chosen.

Pump curve (Source: Moyno)

Use appropriate HP and pressure scales for the number of stages required.

NOTE: Pressure limits rated at 87 psi/stage (70 Duro.) Some models have additional limits. Please consult factory before making final selection.

		RPM	100	200	300	400	500
	NPSH Required — (Ft.)		1.5	3.0	5.0	9.0	12.0
Minimum Recommended Motor HP		1 STG	3	5	7½	10	10
		2 STG	5	7½	15	15	20
		4 STG	7½	15	25	30	40
		6 STG	15	30	40	50	60
Drive End HP Must be added to HP value from curve.		F	.26	.51	.76	1.01	1.27
		G	0.37	0.73	1.10	1.47	1.83
		H	0.57	1.13	1.70	2.27	2.83
		J	0.67	1.33	2.00	2.67	3.33
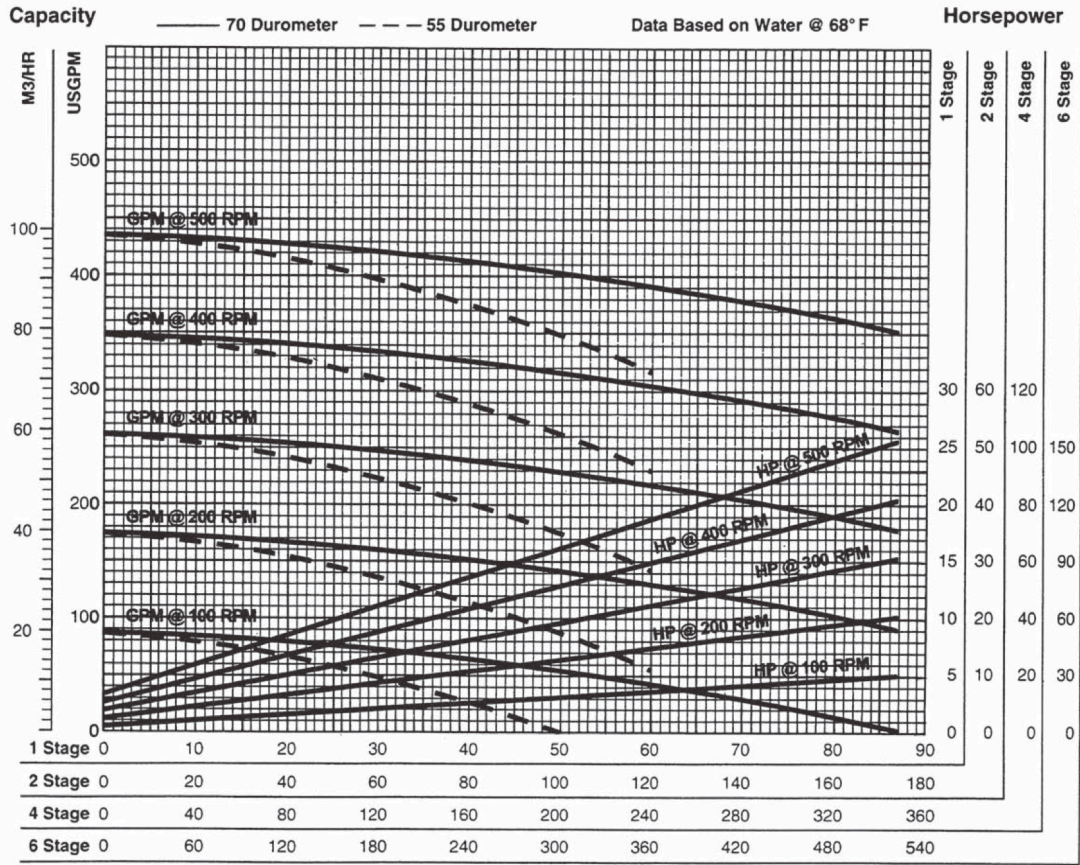
Differential Pressure (PSI)*

*(PSI x .069 = BAR) (PSI x .070 = kgf/cm²) (USGPM x .2271 = M³/HR) (HP x .746 = kW)

Trough Description and photograph:

Trough dimensions: 1829mm X 762mm X 406mm. The trough was used as a storage container for the slurry flushed out from the pipe loop. It was designed with three compartments so that the solids from the incoming slurry stream settle mostly in the first compartment. The water would then overflow from the first compartment into the next two compartments. Water in the third compartment is then drained into the floor drain through an exit hose attached at the bottom of the third compartment. The solids in the first compartment were shoveled out for re-use or disposal.

Appendix F: Linear velocity calculation in the hypothetical liquid CO_2 slurry pipeline

Basis: Available mass flow rate = 2 million tonnes of liquid CO_2 per year

Assuming density of liquid CO_2 to be 867 kg/m^3:

$$Volumetric\ flow\ rate = \frac{2 * 10^9}{867 * 365 * 24 * 3600} = 0.0731 m^3/s$$

With 8" pipe, linear flow velocity, V, is as follows:

$$V = \frac{0.0731}{3.14 * 0.25 * 0.2 * 0.2} = 2.33 m/s$$